学 位 論 文

Study on the regulatory function of Annexin A1 (AnxA1) in pathological bone resorption and its therapeutic implications in periprosthetic osteolysis

(アネキシンA1 (AnxA1) の病的骨吸収制御メカニズム及び人工関節周囲骨吸収における治療効果に関する研究)

２０２２年９月

北 海 道 大 学

Terukawa Hend (Hend Alhasan)

照川 ヘンド

学 位 論 文

Study on the regulatory function of Annexin A1 (AnxA1) in pathological bone resorption and its therapeutic implications in periprosthetic osteolysis

(アネキシンA1 (AnxA1) の病的骨吸収制御メカニズム及び人工関節周囲骨吸収における治療効果に関する研究)

２０２２年９月

北 海 道 大 学

Terukawa Hend (Hend Alhasan)

照川 ヘンド

Table of Contents

List of publications and presentations

Scientific articles

Graduation article

[1] Alhasan H, Terkawi MA, Matumae G, Ebata T, Tian Y, Shimizu T, Nishida Y, Yokota S, Garcia-Martin F, Abd Elwakil MM, Takahashi D, Younis MA, Harashima H, Kadoya K. Iwasaki N. Inhibitory role of annexin A1 in pathological bone resorption and its therapeutic implications in periprosthetic osteolysis. Nature Communications. 2022 Jul 7;13(1):3919.

Other articles

[1] Yokota S, Shimizu T, Matsumae G, Ebata T, Alhasan H, Takahashi D, Terkawi MA, Iwasaki N. Inflammasome Activation in the Hip Synovium of Rapidly Destructive Coxopathy Patients and Its Relationship with the Development of Synovitis and Bone Loss. Am J Pathol. 2022 May;192(5):794-804. doi: 10.1016/j.ajpath.2022.02.003. Epub 2022 Mar 12. PMID: 35292262.

[2] Matsumae G, Kida H, Takahashi D, Shimizu T, Ebata T, Yokota S, Alhasan H, Aly MK, Yutani T, Uetsuki K, Terkawi MA, Iwasaki N. Determination of optimal concentration of vitamin E in polyethylene liners for producing minimal biological response to prosthetic wear debris. J Biomed Mater Res B Appl Biomater. 2022 Jul;110(7):1587-1593. doi: 10.1002/jbm.b.35019. Epub 2022 Feb 5. PMID: 35122380.

[3] Yokota S, Matsumae G, Shimizu T, Hasegawa T, Ebata T, Takahashi D, Heguo C, Tian Y, **Alhasan H**, Takahata M, Kadoya K, Terkawi MA, Iwasaki N. Cardiotrophin Like Cytokine Factor 1 (CLCF1) alleviates bone loss in osteoporosis mouse models by suppressing osteoclast differentiation through activating interferon signaling and repressing the nuclear factor-κB signaling pathway. Bone. 2021 Dec;153:116140.

[4] Matsumae G, Shimizu T, Tian Y, Takahashi D, Ebata T, **Alhasan H**, Yokota S, Kadoya K, Terkawi MA, Iwasaki N. Targeting thymidine phosphorylase as a potential therapy for bone loss associated with periprosthetic osteolysis. Bioeng Transl Med. 2021 Jun 8;6(3):e10232.

[5] Ebata T, Terkawi MA, Hamasaki M, Matsumae G, Onodera T, Aly MK, Yokota S, **Alhasan H**, Shimizu T, Takahashi D, Homan K, Kadoya K, Iwasaki N. Flightless I is a catabolic factor of chondrocytes that promotes hypertrophy and cartilage degeneration in osteoarthritis. iScience. 2021 May 24;24(6):102643.

[6] Tian Y, Terkawi MA, Onodera T, **Alhasan H**, Matsumae G, Takahashi D, Hamasaki M, Ebata T, Aly MK, Kida H, Shimizu T, Uetsuki K, Kadoya K, Iwasaki N. Blockade of XCL1/Lymphotactin Ameliorates Severity of Periprosthetic Osteolysis Triggered by Polyethylene-Particles. Front Immunol. 2020 Aug 4;11:1720.

[7] Hamasaki M, Terkawi MA, Onodera T, Tian Y, Ebata T, Matsumae G, **Alhasan H**, Takahashi D, Iwasaki N. Transcriptional profiling of murine macrophages stimulated with cartilage fragments revealed a strategy for treatment of progressive osteoarthritis. Sci Rep. 2020 May 5;10(1):7558.

[8] Terkawi MA, Kadoya K, Takahashi D, Tian Y, Hamasaki M, Matsumae G, **Alhasan H**, Elmorsy S, Uetsuki K, Onodera T, Takahata M, Iwasaki N. Identification of IL-27 as potent regulator of inflammatory osteolysis associated with vitamin E-blended

ultra-high molecular weight polyethylene debris of orthopedic implants. Acta Biomater. 2019 Apr 15;89:242-251.

Presentations in scientific meeting and conferences

International

[1] ORS 2022. **Alhasan H**, Terkawi MA, Abd Elwakil MM, Matsumae G, Ebata T, Nishida y, Shimizu S, Takahashi D, Harashima H, Iwasaki N. Injectable thermosensitive hydrogel containing N-terminal AnxA1 A2-26 peptide for local treatment of pathological bone resorption associated with inflammation. Orthopaedic Research Society Annual Meeting Feb 4-8, 2022, Tampa Convention Center Tampa, Florida, USA. Poster presentation.

[2] ORS 2021. **Alhasan H**, Terkawi MA, Matsumae G, Ebata T, Takahashi D, Shimizu T, Yokota S, Kadoya K, Iwasaki N. Annexin A1 (AnxA1) for potential therapeutic and translatable intervention in bone diseases typified by pathological bone resorption. Orthopaedic Research Society Annual Meeting Feb 12-16, 2021. Oral presentation.

[3] ORS 2020. **Alhasan H**, Ebata T, Terkawi MA, Tian Y, Matsumae G, Hamasaki H, Takahashi D, Shimizu T, Kadoya K, Iwasaki N. Neutrophils-derived annexin A1 is a potential regulator of inflammatory osteolysis triggered by polyethylene wear debris of orthopedic implants. Orthopaedic Research Society Annual Meeting Feb 8-11, 2020. Phoenix Convention Center Phoenix, Arizona. Poster presentation.

[4] ORS 2019. **Alhasan H**, Terkawi MA, Tian Y, Matsumae G, Hamasaki M, Takahashi D, Ebata T, Kadoya K, Iwasaki N. The crucial role of neutrophils in resolution of inflammatory osteolysis elicited by polyethylene wear debris of orthopedic

prosthetics. Research Society Annual Meeting. Austin, Texas, USA. Feb 2 – 5, 2019. Poster presentation.

Domestic

[1] The 140th Hokkaido Society of Orthopaedics and Traumatolog. **Alhasan H**, Terkawi MA, Matsumae G, Ebata T, Takahashi D, Shimizu T, Yokota S, Kadoya K, Iwasaki N. Annexin A1 activates PPARG signaling and suppresses inflammatory osteolysis and bone resorption. Jun 5-6, 2021. Society Meeting. Asahikawa Medical University Department of Orthopedic Surgery. Oral presentation.

[2] The 36th Annual Meeting of the Japanese Orthopedic Association. **Alhasan H**, Terkawi MA, Matsumae G, Ebata T, Takahashi D, Shimizu T, Yokota S, Kadoya K, Iwasaki N. Annexin A1 (AnxA1) suppresses inflammatory osteolysis and bone resorption through activating PPARG signaling. Oct 14-15, 2021. Mie University. Oral presentation.

[3] The 34th Annual Research Meeting of the Japanese Orthopaedic Association. **Alhasan H**, Terkawi MA, Tian Y, Matsumae G, Hamasaki M, Takahashi D, Ebata T, Kadoya K, Iwasaki N. Neutrophils-derived ANXA-1 inhibits osteoclastogenesis triggered by polyethylene wear particles of orthopedic implants. Yokohama, Japan. October 18, 2019. Oral presentation.

[4] 136th Hokkaido Society of Orthopaedics and Traumatology. **Alhasan H**, Terkawi MA, Tian Y, Matsumae G, Hamasaki M, Takahashi D, Kadoya K, Iwasaki N. Neutrophils-derived ANXA1 inhibits osteoclastogenesis triggered by polyethylene wear debris of orthopedic implants. Sapporo, Japan. January 27, 2019. Oral presentation.

1. Summary

Background and purpose

Total joint arthroplasty (TJA) is the most prosperous approach that reduces pain and restores the function of joint in patients worldwide. Periprosthetic osteolysis associated pathological bone resorption is the most common cause of arthroplasty failure. Wear debris derived from implant during the motion of the joint triggers local inflammatory response followed by pathological bone resorption resulting in mechanical instability of prosthetic components. Therapeutic targets, including bisphosphonates and monoclonal antibodies to receptor activator of nuclear factor kappa-B ligand (RANKL), tumor necrosis factor-alpha (TNF-α) or interleukin-1 (IL-1) that reduce osteoclastic-bone resorbing activity or block inflammation have failed to prevent pathological bone loss or to prolong the lifespan of implant. A better understanding of molecular and cellular mechanisms is necessary for development of novel therapeutic intervention. Macrophages play a vital role in the pathogenesis of osteolysis, as they are the predominant cells at the site of periprosthetic tissues, major source of inflammatory cytokines and they can be differentiated into osteoclasts. My earlier study showed that depletion of neutrophils resulted in greater osteolytic lesions induced by wear debris which were associated with significant reduction in gene expression of AnxA1 in calvarial bone, suggesting a regulatory potential role in periprosthetic osteolysis. Thus, the objective of the current research is to explore molecular function of AnxA1 in periprosthetic osteolysis as a step towards development therapeutic intervention.

Materials and Methods

Freshly isolated human neutrophils were cultured with particulate debris of implant bearing materials of conventional cross-linked ultra-high molecular weight polyethylene

debris (UHMWPE) for 2 h and then harvested for cytokine quantification and gene expression analysis and Western blotting. Murine debris induced-calvarial osteolysis model was used for in vivo evaluation. *AnxA1*-deficient mice and function blocking antibody were used to explore the function of AnxA1 in inflammatory osteolysis. For treatment experiment, following implantation of UHMWPE debris (6 mg), mice were injected onto their calvarial bone with 5 injections of N-terminal AnxA1 (Ac2-26), or 3 injections of FPR2 antagonist (WRW4). A group of mice were treated by Ac2-26 after implantation of UHMWPE debris and interperitoneally injected (5 times in parallel to Ac2-26) with PPAR-γ antagonist (GW9662). Calvariae were collected on day 7 for evaluation of lesions in bone tissues. Consecutive injections of RANKL (non-inflammatory osteolysis model) or TNF-α (inflammatory osteolysis model) for 4 days at concentration of 100 μg/kg were performed onto calvarial bone to induce calvarial osteolysis models. Changes in calvariae were analyzed by high-resolution micro-computed tomography assessment (μCT) and histopathology. For histology and histomorphometry, 10% formalin-fixed calvariae were decalcified in 10% EDTA for 1 week and embedded in paraffin. Five-micron sections were stained with HE and TRAP staining. An injectable thermosensitive hydrogel containing AnxA1 A2-26 peptide was prepared for treatment of pathological bone resorption associated with inflammation. Image J software was used for quantitative analyses. Significant difference between the groups was determined by one-way ANOVA, followed by Tukey's multiple-comparison procedure. Human monocytes were cultured growth medium supplemented with recombinant macrophage colony-stimulating factor (MCSF) plus RANKL with or without recombinant AnxA1 for osteoclast and bone resorption assays. Next, the transcriptional profiling of stimulated cells for 8 days was analyzed by RNA sequencing.

Results

To gain an insight into the molecular response of neutrophils to wear debris, gene expression of human neutrophils stimulated by UHMWPE debris for 2 h were analyzed. Notably, stimulated neutrophils exhibited significant upregulation of AnxA1 but not IL-10 or TGF-β. Consistently, AnxA1 was detected in synovial fluids collected from three patients undergoing revision surgery due to aseptic loosening. It is worth mentioning that the greater osteolytic lesions in neutrophil-depleted mice were associated with significant reduction in gene expression of AnxA1 in calvarial bone. In *AnxA1*-defecient mice, the osteolytic lesions were more severe than these in the wild type mice, suggesting the regulatory role of AnxA1 in pathological bone resorption associated with periprosthetic osteolysis. Furthermore, recombinant Anxa1 inhibited the differentiation of osteoclasts and reduced inflammatory responses of macrophages *in vitro*. RNA-seq data and bioinformatics revealed that treatment of macrophages with AnxA1 suppressed activation of NF-κB signaling pathway and promoted the expression of genes involved in PPAR-γ pathway. To assess therapeutic application of AnxA1 for treating periprosthetic osteolysis, UHMWPE particles were implanted onto calvarial bone tissues followed by consecutive 5 local injections of N-terminal AnxA1 (Ac2-26) over 5 days. Notably, administration of Ac2-26 mimetic peptide onto calvariae significantly reduced bone loss, inflammatory cells infiltrate, and osteoclast-stained areas (TRAP) triggered by UHMWPE debris. In contrast, WRW4 treatment exaggerated osteolytic lesions induced by UHMWPE debris. Interestingly, the therapeutic effects of Ac2-26 were abrogated in mice received GW9662, suggesting that there is correlation between therapeutic mechanism of AnxA1 and PPAR-γ pathway activation. Together, these data demonstrated that AnxA1/PPAR-γ axis may play regulatory role in attenuating inflammation and pathological bone resorption induced

by implant wear debris. To further gain a better insight into the mechanism of action of AnxA1 in pathological bone resorption, TNF-α- and RANKL-induced bone loss models were used. Remarkably, Ac2-26 peptide treatment resulted in significant reduction in bone loss, inflammatory cells infiltrate, and osteoclast-stained areas in the two osteolysis models. Likewise, a single administration of the Ac2-26-mixed Matrigel onto calvariae (beyond lambdoid suture) suppressed the osteolytic lesions and the pathological bone resorption induced by the TNF-α administrations.

Discussion

Chronic inflammation occurred at the site of implant plays crucial role is this pathological condition as it negatively affects bone metabolism and promotes bone resorption resulting in a loss of implant fixation. There is a growing body of evidence suggesting that controlling chronic inflammation at the implant site would be a promising approach for therapeutic intervention. AnxA1 is an endogenous pro-resolving mediator that is abundantly expressed in inflammatory exudates with the potential for serving as a therapy for a variety of inflammatory diseases. This study highlights AnxA1 as clinically-translatable therapeutic agent for managing diseases typified by pathological bone resorption. Macrophages treated by AnxA1 exhibited elevation in the expression of PPARγ and reduction in NFκB signaling pathway. In line with these findings, activation of PPARγ has been reported as promising approach for treatment of inflammatory diseases and cancer through reducing NFκB p65 transcriptional activity. In fact, activation of PPARγ derives polarization of monocytes to M2 macrophages with anti-inflammatory properties and inhibits RANKL- and TNF-α-mediated osteoclast differentiation. In analogous fashion, IL-4 inhibits RANKL-induced osteoclast formation though suppressing NF-κB activation mediated by PPARγ. Therefore, the possible

inhibitory effects of AnxA1 on inflammation and osteoclast differentiation might be due to its ability to decrease activation of NF-κB signaling which is known as positive regulator of pro-inflammatory function of macrophages and bone resorbing function of osteoclasts. These results revealed that AnxA1/PPARγ axis seems to play an important role in attenuating inflammation and pathological bone resorption.

Conclusions

The present study sheds a light for the first time on the functional and cellular associations between neutrophils and pathophysiology of inflammatory osteolysis, delineating new strategies for innovative therapeutic approaches for prevention of implant failure. AnxA1/PPARγ axis seems to play an important role in attenuating inflammation and pathological bone resorption in periprosthetic osteolysis. The safety and efficacy of AnxA1 make it a novel clinically-translatable therapeutic agent for prevention of implant loosening.

2. List of abbreviations

TJA	Total joint arthroplasty
UHMWPE	Ultra-high molecular weight polyethylene
VEUHMWPE	Vitamin E blended ultra-high molecular weight polyethylene
FBS	Fetal bovine serum
αMEM	Modification of Minimum Essential Medium
PBS	Phosphate buffered saline
TBS	Tris-buffered saline buffer
HRP	Horseradish peroxidase
PMA	Phorbol myristate acetate
qRT–PCR	Quantitative real-time polymerase chain reaction
TNF-α	Tumor necrosis factor
RANKL	Receptor activator of nuclear factor kappa-B ligand
IL-1	Interleukin 1
IL-18	Interleukin 18
IL-10	Interleukin 10
IL-4	Interleukin 4
IL-6	Interleukin 6
IL-8	Interleukin 8
AnxA1	Annexin A1
TGFβ	Transforming growth factor beta
NLRP3	NOD-, LRR- and pyrin domain-containing protein 3

NFκB	Nuclear factor κB
ROS	Reactive oxygen species
NADPH	Oxidases NOXs
EVs	Extracellular vesicles
CTSK	Cathepsin K
TRAP	Tartrate-resistant acid phosphatase
ACP5	Tartrate-resistant acid phosphatase
GAPDH	Glyceraldehyde 3-phosphate dehydrogenase
MPO	Myeloperoxidase
P65	RELA NF-kappa-B p65 subunit
P105	Nuclear factor NF-kappa-B p105 subunit NFKB1
RELB	ELB Proto-Oncogene, NF-KB Subunit
PPARγ	Peroxisome Proliferator Activated Receptor Gamma
IFN-γ	Interferon gamma
RUNX2	Runt-related transcription factor 2
COL1A	Collagen Type I Alpha 1 Chain
VEGFA	Vascular Endothelial Growth Factor A
MMP1	Matrix metalloproteinase-1
MMP3	Matrix metalloproteinase-3

3. Introduction

Total joint arthroplasty (TJA) is the most reasonable approach of orthopedic surgeons that restores the function of end-stage arthritic joints. The first successful TJA was performed in 1961 by Dr. John Charnley, and since that time, millions of patients are receiving TJA namely knee and hip arthroplasties every year (Charnley J, 1961). Since that time, intensive efforts have been made to advance device technologies and improve practical procedures and lead to a dramatic increase in survival rate of TJA and prolong in lifespan of implant. Nonetheless, aseptic loosening following periprosthetic inflammatory osteolysis remains the leading cause of arthroplasty failure, a condition typically requires urgent revision surgery (Kandahari AM et al., 2016). It is expected that number of revision surgery due to aseptic loosening will raise with an increase of primary TJA in young patients who are supposed to be more active and to live longer life than older patients. Revision surgery represents a significant challenge to orthopedic surgeons in terms of procedures and consequent complications. In fact, the annual economic burden associated with this surgery is estimated to exceed 3 billion dollars in the USA. These together point to the need for a new therapeutic intervention to extend the lifespan of a prosthesis (Bala A et al., 2019).

Prosthetic wear particulate debris released from materials derived from prosthetic components are believed to be the leading cause of periprosthetic osteolysis (Cobelli N et al., 2011. Deposition of debris in tissues induces a chain biological reaction leading to the formation of a hostile inflammatory environment that favors bone-resorbing activity of osteoclasts, thereby resulting in local bone loss and loosening of the prosthesis. Specifically, debris activate immune cells that initiate biological reactions typified by the

activation of damage-associated molecular patterns, Toll-like receptor signaling, the activation of NLRP3 inflammasomes and nuclear factor κB (NFκB), resulting in the production of pro-inflammatory cytokines, including IL-1β, IL-18, TNF-α, and the formation of granuloma around the prostheses (Kandahari AM et al., 2016). The progressive inflammatory environment at the site of an implant impairs bone metabolism and promotes osteoclastogenesis and bone resorption resulting in a loss of implant fixation (Cobelli N et al., 2011; Kandahari AM et al., 2016). Nonetheless, therapeutic agents reducing inflammation or osteoclastic-bone resorbing activity have failed to prevent pathological bone loss or prolong the lifespan of implant (Terkawi MA et al., 2022). Thus, there is a growing consensus that development of effective treatment for osteolysis needs a better understating of the pathophysiological mechanism of the disease at cellular and molecular level (Terkawi MA et al., 2018).

Macrophages are thought to play a crucial role in the pathogenesis of osteolysis, as they are the predominant cells at the site of periprosthetic tissues that produce inflammatory cytokines and form precursor of osteoclasts in bone tissues. Moreover, other infiltrated cells including fibroblasts, dendritic cells, and neutrophils have been also implicated in the pathogenesis of osteolysis (Ito S et al., 2009; Wozniak W et al., 2004; Papatheofanis FJ & Barmada R, 1991). Of these, neutrophils that are the most abundant circulating leukocytes in the blood and are originates from myeloid precursors within the bone marrow through the myeloblast–promyelocyte–myelocyte–metamyelocyte pathway. They are professional phagocytic cells that play essential role in our defense system. They are highly motile cells and rapidly migrate to infected sites, where they recognize and eliminate the pathogens via NADPH oxidase-dependent mechanisms and their lytic

enzyme activity. However, overactivated neutrophils trigger severe pathological processes typified by the secretion of excess levels of inflammation cytokines and ROS, and the massive formation of NETosis (Nathan C, 2006; Németh T & Mócsai A, 2012; Mócsai A, 2013). On the other hand, neutrophils have another important function in tissue through secreting pro-resolution products and reprogramming macrophages towards the regulatory phenotype leading to resolution of inflammation in the joints (Headland SE et al., 2015; Rhys HI et al., 2018; Schauer C et al., 2014). These issues together raise an important question of how neutrophils function in periprosthetic osteolysis (Wozniak W et al., 2004; Papatheofanis FJ & Barmada R, 1991).

Given the importance of understanding the role of neutrophils in the pathophysiology of periprosthetic osteolysis as a step toward discovering new therapeutic agents, I studied in my master course the functional role of neutrophils in pathogenesis of periprosthetic osteolysis using a murine wear debris-induced osteolysis model. My results demonstrated that administration of Ly6G monoclonal antibody for neutrophil depletion resulted in elevated osteolytic activity induced by wear debris, suggesting that neutrophils play a regulatory role in periprosthetic osteolysis. The immunosuppressive role of neutrophils has been noted in other inflammatory diseases through the production of pro-resolving mediators that control inflammatory responses in dendritic cells, monocytes, macrophages, and T helper type 1 cells (Moutsopoulos NM et al., 2014; Nadkarni S et al., 2016). Generally, upon activation of neutrophils, they can turn off the production of pro-inflammatory cytokines and launch an anti-inflammatory transcriptional program characterized by the release of TGF-β and other specialized pro-resolving mediators. Moreover, neutrophils control inflammation through releasing extracellular vesicles that

restrict the inflammatory activation and polarization of macrophages and extracellular traps that limit inflammation caused by cytokines and chemokines (Rhys HI et al., 2018; Schauer C et al., 2014; Moutsopoulos NM et al., 2014; Nadkarni et al., 2016). Therefore, the increases in the numbers of infiltrated inflammatory cells into calvarial lesions and the extent of inflammation in neutrophil-depleted mice observed in earlier study might be due to a lack of pro-resolving factors of the neutrophils which would limit macrophage infiltration and regulate pro-inflammatory mediators. These actions might lead to the recruitment of more macrophages that could be differentiated into bone-resorbing osteoclasts at the site of inflammation resulting in increased bone resorption.

There is a growing body of evidence to suggest that controlling chronic inflammation at the site of an implant would be a promising approach for therapeutic intervention (Terkawi MA et al., 2022). Chronic inflammation generally occurs when the initial acute inflammation is not effectively resolved due to the inadequate pro-resolving activity of immune system, a process that is referred to as frustrated resolution. The resolution of inflammation is an active process that is rigidly orchestrated by endogenous pro-resolving mediators that function not as immunosuppressive agents, but instead they promote the resolution of inflammation though activating homeostatic control mechanisms in the affected tissues (Fullerton J, Gilroy D, 2016). Of these molecules, Annexin A1 (AnxA1), a member of the annexin superfamily that is mainly released by monocytes and neutrophils, has been implicated in number of biological processes, including inflammation, intracellular vesicle trafficking, leukocyte migration, and tissue growth and regeneration, and apoptosis (Buckley C D et al., 2014; Perucci LO et al., 2017; Gavins FN, Hickey MJ, 2009). In fact, the ability of AnxA1 to stimulate endogenous pro-

resolving pathways leading to tissue repair and healing and its therapeutic effects have been documented in a broad range of experimental models, including myocardial ischemia injury, stroke, sepsis, arthritis, and multiple sclerosis (Perretti M, Dalli J. 2009; Kao W, et al., 2014). Given that periprosthetic osteolysis is a chronic inflammatory disorder typified by persistent inflammation, and that pro-resolving mediators may restore tissue homeostasis, we explored the function of AnxA1 in the pathophysiology of disease and evaluated its therapeutic applications in experimental periprosthetic osteolysis models.

4. Methods

4.1.Ethical approvals of the study

The research protocols for the use of human samples were approved by the Research Ethics Review Committee of Hokkaido University Hospital (Approval ID: 016-0002). Informed consents were obtained from all donors. Animal experiments were performed in accordance with our approved protocols (nos. 17-0085 & 18-0171) by the Institute of Animal Care and Use Committee of the Hokkaido University Graduate School of Medicine.

4.2.Immunostaining of synovial tissues

Formalin-fixed synovial tissues from three patients (one male of 60-year old, two females of 54- and 59-year old) undergoing revision of total hip arthroplasty were embedded in paraffin and 3 μm sections were used for immunohistochemistry staining (IHC). All samples didn't show any clinical signs of local infection with level of serum CRP below 0.07 mg/dl. Control tissue was collected from patient of hip osteoarthritis (female 64-year old) undergoing primary hip arthroplasty. Sections were deparaffinized, treated for 5 min with proteinase K (Dako, CA, USA) for antigen retrieval, and then blocked with horse serum for 1 h. Sections were incubated with primary antibodies to myeloperoxidase (MPO: Novus Biologicals, USA), neutrophil Elastase (Abcam, Cambridge, UK), CD68 (Dako Agilent, USA), and AnxA1 (Biolegend, San Diego, USA) overnight at a concentration of 1:200 and then washed three times with tris-buffered saline buffer (TBS). The signal was amplified with horseradish peroxidase (HRP)-conjugated streptavidin secondary antibody (Vectastain Elite ABC kit; Vector Laboratories,

Burlingame, USA) followed by counterstaining with hematoxylin for detecting cellular nuclei.

4.3.Wear debris preparation

Fabricated wear particles generated from bearing materials of hip implants of virgin ultra-high molecular weight polyethylene (UHMWPE) or its vitamin E-blended materials (VE-UHMWPE) (Teijin Nakashima medical, Okayama, Japan) were prepared with size range of 0.1-100 µm. The GUR1020 powder (Celanese Japan, Tokyo, Japan) exposed to 95 kGy irradiation and annealed at a temperature below T_m (135 °C) (Quadrant Polypenco Japan, Tokyo, Japan) was used for manufacturing virgin UHMWPE (Terkawi MA et al., 2018). The GUR1050 powder was blended with 0.3 wt% dl-α-tocopherol (Eisai, Tokyo, Japan), exposed to 300 kGy irradiation and then annealed below T_m (135 °C) (Blend-E® XL; Teijin Nakashima medical, Okayama, Japan) was used for manufacturing virgin VE-UHMWPE (Terkawi MA et al., 2019). Thereafter, the manufactured materials were crushed by using a Multi Beads Shocker (Yasui Kikai, Osaka, Japan) at 3500 rpm wand then sterilized using an ethylene oxide gas (EOG) sterilizer (Eogelk-SA-H160, Osaka, Japan). Equivalent circle diameter for particle sizes was determined using the Image analyzer Morphologi G3 (Malvern Instruments, Worcester, UK). Samples were 0.1–100 µm sizes and endotoxin-free as tested using a ToxinSensor Single Test Kit (Genscript, Piscataway, NJ, USA).

4.4.Neutrophil culture and stimulation

Human peripheral blood was collected using BD Vacutainer tubes containing ACD (Becton, Dickinson and Company, NJ, USA) from three healthy Asian donors with no

history of inflammatory diseases, joint disorders and total joint arthroplasty. Human neutrophils were separated by using Ficoll-Paque™ PLUS (GE Healthcare) and then subjected to a MACSxpress neutrophils isolation kit (Miltenyi Biotec., CA, USA). Freshly isolated neutrophils 1×10^6 were seeded onto poly-d-lysine-coated wells and stimulated with UHMWPE debris at a density of 0.1 mg/cm^3 in minimum essential medium Eagle (MEM, Sigma) supplemented with 10% heat-inactivated fetal bovine serum (FBS, Nichirei Biosciences INC, Tokyo, Japan), and 5% mg/L penicillin/streptomycin solution (Wako, Japan) for 2 h at 37 °C in a humidified atmosphere containing 5% CO_2 using inverted culture system (Terkawi MA et al., 2018). For isolation of extracellular vesicles (EVs) of stimulated neutrophils, freshly isolated neutrophils 4×10^6 were stimulated with UHMWPE debris, and the cell suspension diluted in PBS (10 mL total sample volume) was centrifugated at 400 g for 5 min. Supernatant was centrifugated at 2000 g for 10 min, followed by passing through 0.45 µm syringe filter (Advantec INC., CA, USA). EVs were then isolated by ultracentrifugation of supernatant at 100000 g for 1h. Pelleted EVs were washed with PBS and centrifuged again at 100000 g for 1h. The pellet was suspended in 50 µl PBS and then subjected to Western blot analysis.

4.5.Macrophage stimulation and osteoclast differentiation, and their function assays

Human primary monocytes were isolated from the blood samples of healthy donors by density gradient centrifugation (Ficoll-PaqueTM PLUS: GE Healthcare, Waukesha, WI, USA) followed by treatment with a MACS Pan monocyte isolation kit (Miltenyi Biotec, Auburn, CA, USA). The differentiation of macrophages, osteoclasts assay and

bone resorption assay were essentially performed following the standard (Terkawi et al., 2018; Matsumae et al., 2021). Attached cells were cultured in MEM supplemented with 10% heat-FCS, 5% mg/l penicillin/streptomycin solution, and 5% L-glutamine in a 37°C-humidified atmosphere containing 5% CO2 for 3 days in the presence of 25 ng/mL of recombinant macrophage colony stimulating factor (MCSF, Peprotech, NJ, United States). Differentiated macrophages were stimulated with UHMWPE debris in presence or absence of 100 µg recombinant human AnxA1 (R&D Systems, MN, USA) using an inverted culture system. Cultured macrophages were subjected to Western blot analysis (24h stimulation) and TRAP staining (6 days stimulation). Macrophages stimulated with 10 µg/mL recombinant human TNF-α (Peprotech) was used as positive control. In a separate experiment, differentiated macrophages were stimulated with different concentrations of recombinant human AnxA1 (R&D Systems) and harvested at different time points. In addition, cells from a human monocyte cell line THP1 (RIKEN, Saitama, Japan) were seeded at a density of 1×10^5 cells/well onto a 48-well plate and allowed to differentiate into macrophages in the presence of 5 ng/mL phorbol myristate acetate (PMA, Sigma) for 48 h (Yokota S et al., 2021). The cells were next stimulated by treatment with recombinant AnxA1 or synthetic peptide Ac2-26 (KareBay^{TM} Biochem, Inc., NJ, USA). For the preparation of macrophage phenotypes, the cells were stimulated for 48 h with a 100 ng/mL solution of lipopolysaccharide (LPS; Sigma) plus a 100 ng/mL solution of recombinant human interferon gamma (IFN-γ) for M1 macrophages and 200 ng/mL IL-4 (Peprotech) for M2 macrophages (Yokota S, et al., 2021). For osteoclast differentiation, monocytes were cultured in medium supplemented with 25 ng/mL MCSF and 50 ng/mL RANKL (Peprotech) plus different concentrations of recombinant human AnxA1 (R & D systems). Cells were stained on day 8 using a TRAP kit (Sigma) and

TRAP-positive stained cells with ≥ 3 nuclei were counted as the osteoclasts. Bone pits on dentine slices were detected by staining with 20 mg/mL of a solution of peroxidase-conjugated wheat germ agglutinin and 3,3'-diaminobendzidine (0.52 mg/mL in PBS containing 0.1% H_2O_2) on day 21 (Terkawi et al., 2019). Slices were examined using a confocal microscope and pits were calculated as the percentage of resorbed bone surface/total bone surface area (ImageJ, NIH).

4.6.Fibroblast-like synoviocytes (FLS) and osteoblast stimulation

The hFLS from normal healthy human synovial tissues purchased from Cell Applications (Cell Applications) were cultured according to the supplier's recommendations. Cultured cells were stimulated with UHMWPE debris at a density of 0.1 mg/cm^3 for 24 h at 37 °C in a humidified atmosphere containing 5% CO_2 using inverted culture system. In a separated experiment, cultured hFLS cells were stimulated with recombinant human TNF-α (Peprotech) in the presence or absence recombinant AnxA1 (R&D Systems). On the other hand, human fetal osteoblasts purchased from Cell Applications (San Diego, CA, USA) were cultured in osteoblast growth medium (Cell Applications). Cells were differentiated in osteoblast differentiation medium (Cell Applications) for 14 days and cultures were regularly replenished with fresh media every 3 days (Tian Y, et al., 2020). Cells were stimulated with either recombinant human TNF-α (Peprotech) for 48h in the presence or absence recombinant AnxA1 (R&D Systems).

4.7.Western Blotting

Proteins of lysed cells were separated in SDS-PAGE gels by electrophoresis and then transferred to polyvinylidene fluoride membrane (Immobilon-P Membrane; Merck,

Darmstadt, Germany). Primary antibodies to β-actin (Abcam, UK), AnxA-1 (Biolegend), MPO (Novus Biologicals), total NFκB P65 (Biolegend), phospho NFκB P65, phospho NFκB P105, phospho P38, phospho RelB and PPAR-γ (Cell signaling technology, CST, MA, USA). Respective secondary antibodies conjugated with HRP were used for detection of bound antibodies (CST). Signals were detected by Ez WestLumi Plus (ATTO, Tokyo, Japan) and bands were visualized using a Quantity One v. 4.6.9 (Bio-Rad) software. Bands were quantified for relative intensity using ImageJ software (NIH, USA).

4.8.RNA sequencing and bioinformatics

Human monocytes were cultured in growth medium supplemented with recombinant macrophage colony-stimulating factor RANKL plus 100 ng/mL recombinant AnxA1 (R&D systems). We next analyzed the transcriptional profiling of stimulated cells for 8 days by RNA sequencing. An average of 69 million reads (paired-end reads of 101 bp) per sample were mapped by the STAR software and read count was determined using the RSEM software (Matsumae G et al., 2021). Significant differences were calculated using DESeq2 R package (https://www.r-project.org/). Analyses were performed using the Database for Annotation Visualization and Integrated Discovery online tools (DAVID: david.abcc.ncifcrf.gov). Heat map was used to visualize the differences in fold changes in each enriched GO term (http://biit.cs.ut.ee/clustvis/). The RNA-seq data are publicly available at the Gene Expression Omnibus (GEO) database (http: www.ncbi.nlm.nih.gov/geo/) under the accession numbers (GSE183145) and (GSE171542).

4.9.Calvarial debris-induced osteolysis model and osteolytic lesion analysis

Debris-induced osteolysis was induced by implantation of 6 mg fabricated wear of UHMWPE or VE-UHMWPE onto the surface of the calvarial bone of mice for 7 days (Terkawi et al., 2019; Matsumae et al., 2021). Mice were anesthetized by intraperitoneal injection of 100 mg/kg ketamine and 10 mg/kg xylazine. Thereafter, sagittal incision (~1 cm) was made over the calvarial anterior site for implantation of fabricated wear UHMWPE particles (Terkawi MA et al., 2019). The mice were sacrificed after 7 days and their calvariae were subjected to R-mCT2 scan (Rigaku, Tokyo, Japan) for micro-computed tomography assessment (micro-CT). Images were analyzed using ImageJ (NIH, USA) for the quantification of bone loss on the surface of calvariae. For histomorphometry, calvariae were then fixed in 10% of formalin for 48 h, decalcified in a Decalcifying Solution B (FUJIFILM Wako Pure Chemical Corporation, Osaka, Japan) for 3 days, and then embedded in paraffin for conducting the histological examination. The 5 μm-sections were stained with leukocyte acid phosphatase tartrate resistance acid phosphatase (TRAP, Sigma, Tokyo, Japan) and hematoxylin eosin (HE, Wako). The lesions and infiltration of inflammation cells were microscopically examined and analyzed with Image J (NIH).

4.10. Generation of AnxA1-deficient mice (AnxA1 KO)

Generation of AnxA1 KO mice was carried out using CRISPR/Cas9 technique. Briefly, two gRNA targets (5′-GAA CAC CGG TGA TTA CGC TG-3′ and 5′-CTG GCA CTC TTG GTC AGA AG-3′) located on intron 3 and 5 of Anxa1, respectively, were selected for producing the AnxA1 KO mouse in which exons 3 to 5 of the AnxA1 had

been excised. These two gRNAs were synthesized and purified by means of a GeneArt Precision gRNA Synthesis Kit (Thermo Fisher Scientific, Waltham, Massachusetts) and dissolved in Opti-MEM (Thermo Fisher Scientific, Waltham, Massachusetts). Thereafter, the mixture of two gRNAs (25 ng/μL, each) and GeneArt Platinum Cas9 Nuclease (100 ng/μL) were electroplated to the zygotes of C57BL/6J mice (Charles River Laboratories Japan, Yokohama, Japan) by using the NEPA 21 electroporator (Nepa Gene Co. Ltd., Ichikawa, Japan). After electroporation, two cell embryos were transferred into the oviducts of pseudopregnant female and newborns were obtained. Mice were kept under SPF conditions. Genotyping was routinely performed using genomic DNA extracted from <0.5 mm tails of 3–4-week-old mice. PCR was carried out using AmpliTaq Gold 360 Master Mix (Thermo Fisher Scientific, Waltham, Massachusetts) with the appropriate primers (Table 1). The PCR products were purified with a FastGene Gel/PCR Extraction Kit (Nippon Genetics, Tokyo, Japan) and the DNA sequences were obtained using a BigDye Terminator v3.1 Cycle Sequencing Kit (Thermo Fisher Scientific, Waltham, Massachusetts), FastGene Dye Terminator Removal Kit (Nippon Genetics, Tokyo, Japan), and 3500xL Genetic Analyzer (Thermo Fisher Scientific, Waltham, Massachusetts).

Table 1. Primers used for genotyping.

Target region	Sequence
AnxA1 LF	5′-TGTATCCTCGGATGTTGCTG-3′
AnxA1LR	5′-GTAATGGGCTCACGGTGTTT-3′
AnxA1MF	5′-ACAGACGCTCAGTTTGCTCA-3′
AnxA1MR	5′-AACACAAAGCTGCCACATCC-3′

4.11. Treatment procedures in debris-induced osteolysis models

Blocking AnxA1 in vivo was carried out in 8-week-old male C57BL/6 mice using 5μg of a neutralizing mouse monoclonal antibody to AnxA1 (R&D System) that was subcutaneously injected onto calvarial bone at the time of debris implantation and on days 2 and 4 post implantation. Following the same regime, control mice received 5μg of an isotype control antibody (R&D System). For examining the therapeutic effects of AnxA1, eight-week-old male C57/BL6 mice was treated by N-terminal AnxA1 (Ac2-26) or BML111 (R&D Systems) was injected 5 times at concentration of 1 mg/kg. One group of mice were treated with 3 injections of 2.5 mg/kg WRW4 (R&D Systems) on days 1, 3 and 5 post debris implantations. Reagents were dissolved in water and volume and concentrations were adjusted in PBS to 100 μl. Injections were performed subcutaneously onto calvarial bones after implantation of debris. Sham mice and these received PBS injections were considered as controls. In separated experiment, eight-week-old male C57/BL6 mice were treated by 5 subcutaneous injections of Ac2-26. and parallelly 5 intraperitoneal injections of GW9662 (Cayman Chemical, Michigan, USA). GW9662 was dissolved in dimethyl sulfoxide (DMSO) and diluted with PBS to a final concentration of 10%. 1 mg/kg for GW9662 or its solvent (vehicle) was intraperitoneally injected every day for 5 days.

4.12. Cytokines-induced osteolysis model

Murine recombinant RANKL or TNF-α (Biolegend, San Diego, USA) were injected onto the surface of the calvarial bone on 4 consecutive days at concentration of 100 μg/kg. Pathological bone erosions were evaluated on day 7 day for debris-induced osteolysis and

on day 5 for cytokine-induce models using high-resolution micro-computed tomography assessment (micro-CT), histopathology and gene expression (Terkawi MA et al., 2019).

4.13. RNA sequencing and bioinformatics

Human monocytes were cultured in growth medium supplemented with recombinant macrophage colony-stimulating factor RANKL plus 100 ng/mL recombinant AnxA1 (R&D systems). We next analyzed the transcriptional profiling of stimulated cells for 8 days by RNA sequencing. An average of 69 million reads (paired-end reads of 101 bp) per sample were mapped by the STAR software and read count was determined using the RSEM software. Significant differences were calculated using DESeq2 R package (https://www.r-project.org/). Analyses were performed using the Database for Annotation Visualization and Integrated Discovery online tools (DAVID: david.abcc.ncifcrf.gov). Heat map was used to visualize the differences in fold changes in each enriched GO term (http://biit.cs.ut.ee/clustvis/). The RNA-seq data are publicly available at the Gene Expression Omnibus (GEO) database (http: www.ncbi.nlm.nih.gov/geo/) under the accession numbers (GSE183145) and (GSE171542) (Matsumae G et al., 2021).

4.14. Quantitative Real-Time Polymerase Chain Reaction (qRT–PCR).

Cells and tissues were lysed using TRIzol Reagent (Invitrogen) for RNA extraction and cDNAs synthesis using RNeasy Plus Mini kit columns (Qiagen, Hilden, Germany) and GoScriptTM reverse transcriptase kit (Promega, Madison, USA), respectively. SYBR® Premix Ex Taq™ II (Takara, Shiga, Japan) was used for performing qRT-PCR with gene-specific primers (Table 2). Gene expression was calculated by the $2^{-\Delta\Delta Ct}$ method after normalizing to the GAPDH and β-actin (Tian Y et al., 2020).

Table 2. Primers used for gene expression by qRT-PCR.

Target Genes	Forward	Reverse
B actin	CCTCACCCTGAAGTACCCCA	TCGTCCCAGTTGGTGACGAT
hIL-10	GTGTCCGTGAGGTTGGAGGT	AAGGGTTACTTGGGTTGCCA
hTGFβ	CCTGGGGCATCACTTCTACC	TGGAGCTGGTGAAACGGAAG
hAnxA1	TGCACAGCGTCAACAGATCA	CAGTGTTTCATCCAGGGGCT
hRUNX2	TCTCCAGGAGGACAGCAAGA	GCAGCCTTAAATGACTCTGTTGG
hCOL1A	ACTGGCGAAACCTGTATCCG	CCAGTTCTTGGCTGGGATGT
hIL-6	AGAAAAAGGTGGGTGTGTCCT	GTCTTTGAGCCTGTCTTCCCC
hIL-8	TCCAAACCTTTCCACCCCAAA	AATTTCTGTGTTGGCGCAGTG
hVEGFA	AAAACACAGACTCGCGTTGC	CCTCGGCTTGTCACATCTGC
hPPARγ	GGCTACACTGTTCTGCGGAT	CACCCAGATCACAAGCCCAT
mGAPDH	TGCAGCGAACTTTATTGATG	ACTTTGTCAAGCTCATTTCC
mIL-6	TAGTCCTTCCTACCCCAATTTCC	TTGGTCCTTAGCCACTCCTTC
mIL-10	AAGGGTTACTTGGGTTGCCA	CCTGGGGCATCACTTCTACC
mTGF-β	TGGAGCTGGTGAAACGGAAG	CTGGCGAGCCTTAGTTTGGA
mTRAP	TCTTCAGGACGAGAACGGTG	CCTTTCGTTGATGTCGCACA
mCTSK	CAGAAGCAGTATAACAGCAAGG	CCCAAATTAAACGCCGAGAG
mAnxa1	AACCATCGTGAAGTGTGCCA	CTTCGTACAGCTTCTCGGCA
mPPARγ	TGTCTCACAATGCCATCAGGT	CTGGGTTCAGCTGGTCGATA

4.15. Synthesis of Ac2-26 peptide

Peptide Ac2-26 (Ac-AMVSEFLKQARFLENQEQEYVQAVK-NH_2) was synthesized by solid-phase peptide synthesis, purified by semipreparative reverse phase high pressure liquid chromatography (RP-HPLC), and then characterized by MALDI-TOF MS spectrometry and RP-UPLC chromatography. The peptide was obtained as a white amorphous solid (13.45 mg), which was detected by RP-UPLC (t_R 14.175 min, purity 98.11% in the linear gradient from 2% to 60% of CH_3CN (0.1% TFA) in H_2O (0.1% TFA) for 20 min). The calculated m/z was noted as 3026.5417 $[M+H]^+$.

4.16. Preparation of thermo-responsive platform of the peptide

Matrigel® (Corning Inc., USA) was thawed according to the manufacturer's guidelines and kept on ice during the experiments. A 750 μg sample of the lyophilized peptide was dissolved in 50 μL of ultra-pure distilled water and added drop-wise to the Matrigel® solution under vortexing. The resulting hydrogel was immediately either placed on ice or stored at 4 °C until used in further experiments. Aliquots of the prepared hydrogel were diluted in PBS (Wako, Japan) and assayed for the peptide content using a standard BCA assay method (Thermo Fisher scientific, USA). Peptide entrapment efficiency was calculated according to equation: Entrapment efficiency (%) = (Estimated peptide content/theoretical peptide content) × 100. For further evaluating the in vitro release of the hydrogel encapsulating the Ac2-26 peptide, the peptide-containing hydrogel was incubated at 37 °C for few minutes until solidification had occurred, and then incubated in PBS (pH 7.4) in a thermally controlled stirrer (37 °C, 300 rpm). Peptide release was quantified in samples (25 μL) that were frequently at specific time intervals.

For a further understanding of the behavior of the prepared thermo-responsive hydrogel, a kinetic analysis of the release of the peptide from the hydrogel was applied. Linear regression analyses were utilized to fit the peptide release data to the most common models associated with the controlled-release dosage forms, including Zero-order (Equation: $M_t / M_\infty = K_0 t$.), First-order (Equation: $M_t / M_\infty = e^{-K1t}$) and Higuchi-diffusion (Equation: $M_t / M_\infty = k_H t^{½}$). The M_t / M_∞ was the fractional release of the drug at time t, k_0 = Zero-order rate constant, k_1 = First-order rate constant, k_H = Higuchi rate constant and t = time point at which release was estimated. In addition, the equation developed by (Ritger PL and Peppas NA, 1987) was applied to elucidate the mechanism of peptide release from the hydrogel as Equation: $M_t / M_\infty = Kt^n$. The M_t / M_∞ ratio was the fractional release of the drug at time t, K was the release rate constant, and n was the diffusional exponent. In case of hydrogels formed as a thin film sample, n= 0.5 for Fickian diffusion; $0.5 < n < 1$ for non-fickian pattern; n= 1 for case II transport, and $n > 1$ for supercase II transport. These results showed that formulation containing 600 µL Matrigel® achieved a sustain peptide release for one week, with a constant time-independent controlled-release pattern (Table 3 & Table 4). This behavior met criteria needed and is highly favorable for ensuring a sustained therapeutic effect of a drug in vivo.

Table 3. Kinetic analysis of the release of the peptide from the optimum hydrogel at 37 °C and pH 7.4. The average cumulative percentage of the peptide dose released at different time points for three independent experiments was used for the calculation.

Correlation coefficient (r)			Assigned equation		
Zero-order model	First-order model	Higuchi-diffusion model		$t_{50\%}$[a] (hr)	K_{rel}[b]
0.9962	-0.1460	0.9451	$M_t / M_\infty = 0.6057\ t$	82.54	0.6057

[a]$t_{50\%}$: the time required for the release of 50% of the peptide dose.

[b]$K_{rel.}$: release rate constant calculated based on the best-fit kinetic model.

Table 4. Analysis of the peptide release data from the optimum hydrogel at 37 °C and pH 7.4 according to the Ritger and Peppas equation. The average cumulative percentage of the peptide dose released at different time points for three independent experiments was used for the calculation.

n[a]	K[a]	r[b]	Mechanism
1.2426	0.1789	0.9981	Super case-II transport

[a]n and K are the parameters of Ritger and Peppas equation defined in the methods section (Equation 5).

[b]r is the correlation coefficient calculated by linear regression analysis of the Logarithm of cumulative percentage of drug released (Log M_t / M_∞) versus the Logarithm of the corresponding different time points (Log t).

4.17. Statistical analysis.

Analyses were performed using one-way ANOVA followed by Tukey's multiple comparisons procedure and Student *t*-test (GraphPad Software Inc., La Jolla, CA, USA) to compare the differences among groups, and results were considered statistically significant when $p < 0.05$ *, $p < 0.001$**, $p < 0.0001$ ***, $p < 0.00001$ ****. ns indicates no significant difference.

5. Results

5.1. Identification of AnxA1 as a potential regulator of inflammation and pathological bone resorption induced by wear debris.

To understand the molecular response of neutrophils to implant wear particles, freshly isolated human neutrophils were stimulated with ultra-high molecular weight polyethylene (UHMWPE) debris, known as major cause of inflammation after total joint replacement, for 2 h and then subjected to qRT-PCR for analyzing gene expression of pro-resolution-related molecules. Neutrophils stimulated with UHMWPE debris exhibited a significant increase in the expression of AnxA1, but not IL-10 or TGF-β (Figure 1A). Moreover, it should be noted that the greater osteolytic lesions observed in neutrophil-depleted mice were accompanied by a significant decline in the expression of AnxA1, but not IL-10 and TGF-β in calvarial bone tissue (Figure 1B).

Next, I examined it AnxA1 is present in synovium-like tissues (pseudocapsule) and synovial fluids obtained from three patients who received revision surgery after total hip joint replacement. It is noteworthy that AnxA1 was detected in both $CD68^+$ macrophages and $Elastase^+$ neutrophils found in inflammatory areas within pseudocapsule tissues as well as in synovial fluids collected from patients who were undergoing revision surgery due to aseptic loosening (Figure 1C, D). The $CD68^+$ macrophages appeared to be abundant in periprosthetic tissues and only a few $Elastase^+$ neutrophils were detected in these tissues (Figure 1C).

To further assess that the activation of cells by implant wear particles is associated with an increased production of AnxA1, human differentiated macrophages, freshly isolated neutrophils, and fibroblast-like synoviocytes (hFLS) were stimulated with

UHMWPE debris and then subjected Western blot analysis. It should be noted that the expression of AnxA1 did not appear to be significantly increased in macrophages or hFLS stimulated with UHMWPE debris (Figure 2A, B). Given that resident macrophages are heterogenous and that different phenotypes may be present in periprosthetic tissues, the expression of AnxA1 was examined in differentiated inflammatory and anti-inflammatory macrophages. An increase in expression of AnxA1 was found in anti-inflammatory macrophages (M2) that had been stimulated with IL-4 (Figure 1C). It is worth mentioning that neutrophils that had been stimulated with UHMWPE debris exhibited the most significant increase in the expression of AnxA1 in comparison to other type of cells (Figure 2D). Likewise, AnxA1 was further detected in extracellular vehicles of neutrophils (N-EVs) that had been stimulated with UHMWPE debris (Figure 2E). These results suggest that AnxA1 is present in periprosthetic tissues expressed by macrophages and neutrophils and may have a role in the inflammation and pathological bone resorption induced by wear debris.

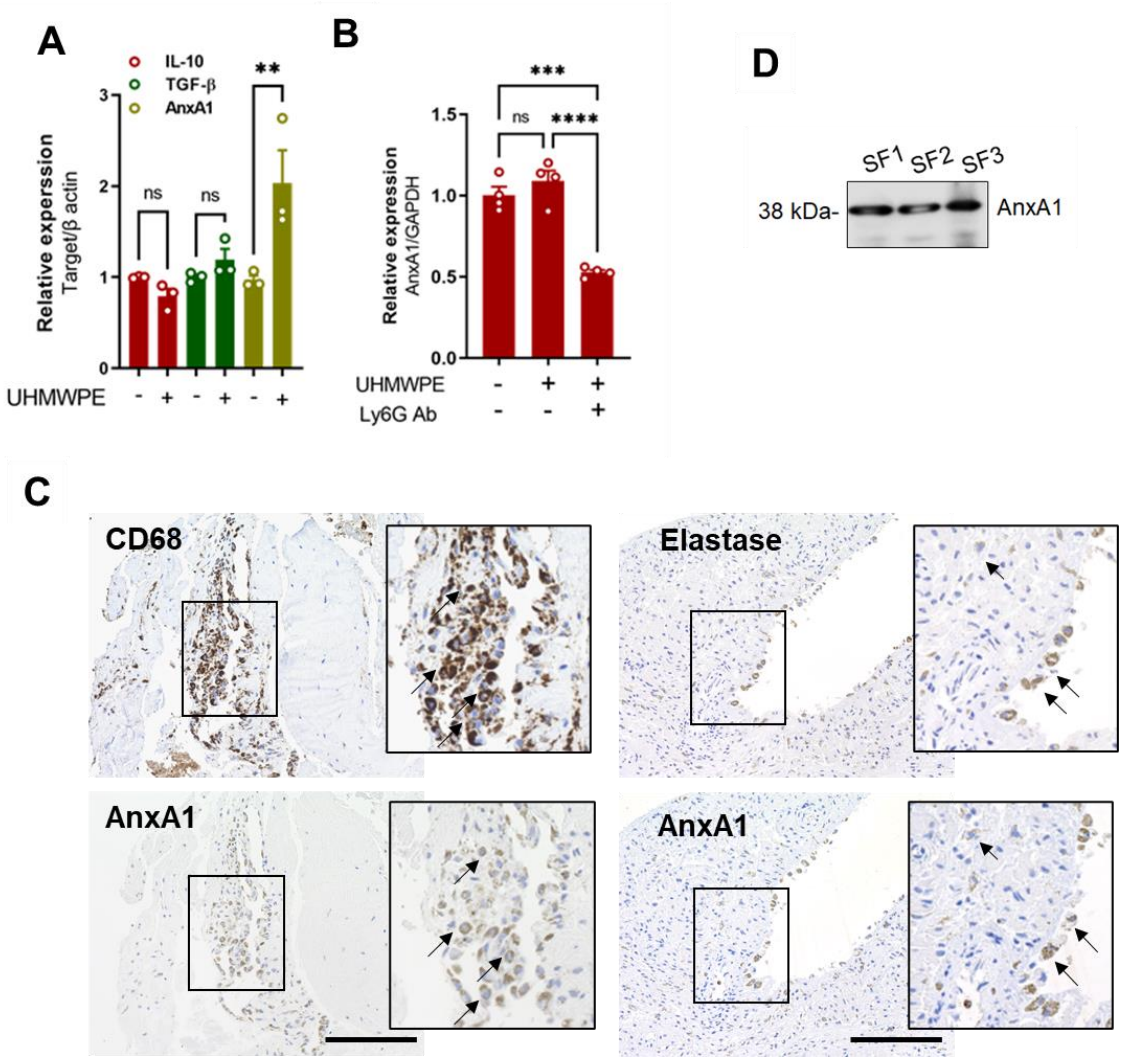

Figure 1. Identification of AnxA1 as a regulator of pathological bone resorption induced by implant debris. A) Gene expression of anti-inflammatory cytokines in human neutrophils stimulated by UHMWPE debris by using qRT-PCR. Results represent the mean for the relative expression values ± SEM of triplicates. **B**) AnxA1 expression in calvarial bone tissues of neutrophil-depleted mice analyzed by qRT-PCR. Results represent the mean of relative expression values ± SEM of 4 mice. **C-D**) Detection of AnxA1 in synovial tissues and fluids (SF) collected from 3 aseptic loosening cases by using Western blotting. Analyzed by IHC. Scale bar is 100µm.

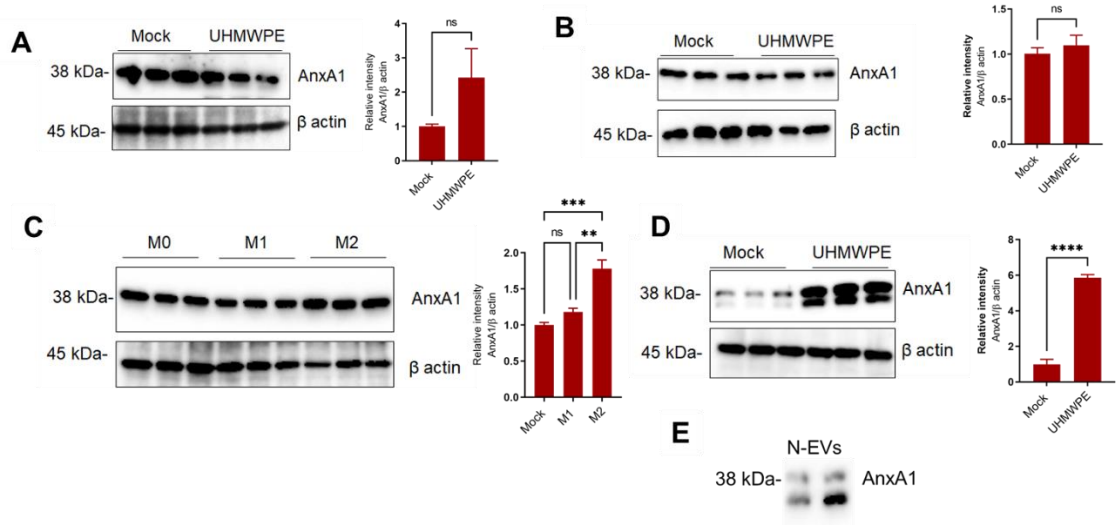

Figure 2. Expression of AnxA1 in cells stimulated with wear debris as analyzed by Western blotting. A) Expression of AnxA1 in stimulated human macrophages with UHMWPE wear debris for 24h. Right panel represents band quantification. B) Expression of AnxA1 in stimulated human FLS. Right panel represents band quantification. C) Expression of AnxA1 in macrophages phenotypes, including in vitro-generated inflammatory M1 (LPS+IFN-γ) and anti-inflammatory M2 (IL-4) cells. Right panel represents quantification of band intensity. D) Expression of AnxA1 in stimulated human neutrophils with UHMWPE wear debris for 2h. Right panel represents quantification of band intensity. Significant difference between the groups was considered when * $p < 0.05$, ** $p < 0.001$, *** $p < 0.0001$, **** $p < 0.00001$.

5.2.The potential regulatory role of AnxA1 is in periprosthetic osteolysis.

To further examine the assumption that AnxA1 plays role in the inflammation and pathological bone resorption induced by wear debris, *AnxA1*-defecient mice were generated and the osteolytic lesions in calvarial bone were evaluated after the implantation of UHMWPE debris. Remarkably, *AnxA1*-defecient mice (*AnxA1* KO) exhibited significantly greater osteolytic lesions with larger TRAP-stained regions in calvarial bone tissues than these in wild-type mice (Figure 3A-C). Consistent with these results, these mice exhibited significant elevations in the expression of inflammatory cytokines, including TNF-α, IL-1β, and IL-6 in granulomatous tissue that was formed around the UHMWPE debris (Figure 3D). Given that AnxA1 is present as a secreted protein or within EVs, we next examined the effects of function-blocking AnxA1 by a specific antibody, which targets secreted AnxA1, on the development of osteolytic lesions in the UHMWPE debris-induced osteolysis model. The local administration of an AnxA1 neutralizing antibody resulted in a significant increase in osteolytic lesions in calvarial bone compared to that in control mice after the implantation of UHMWPE debris (Figure 3E-G). These results suggest that secreted AnxA1 acts as a potential regulator of inflammation and pathological bone resorption in periprosthetic tissues.

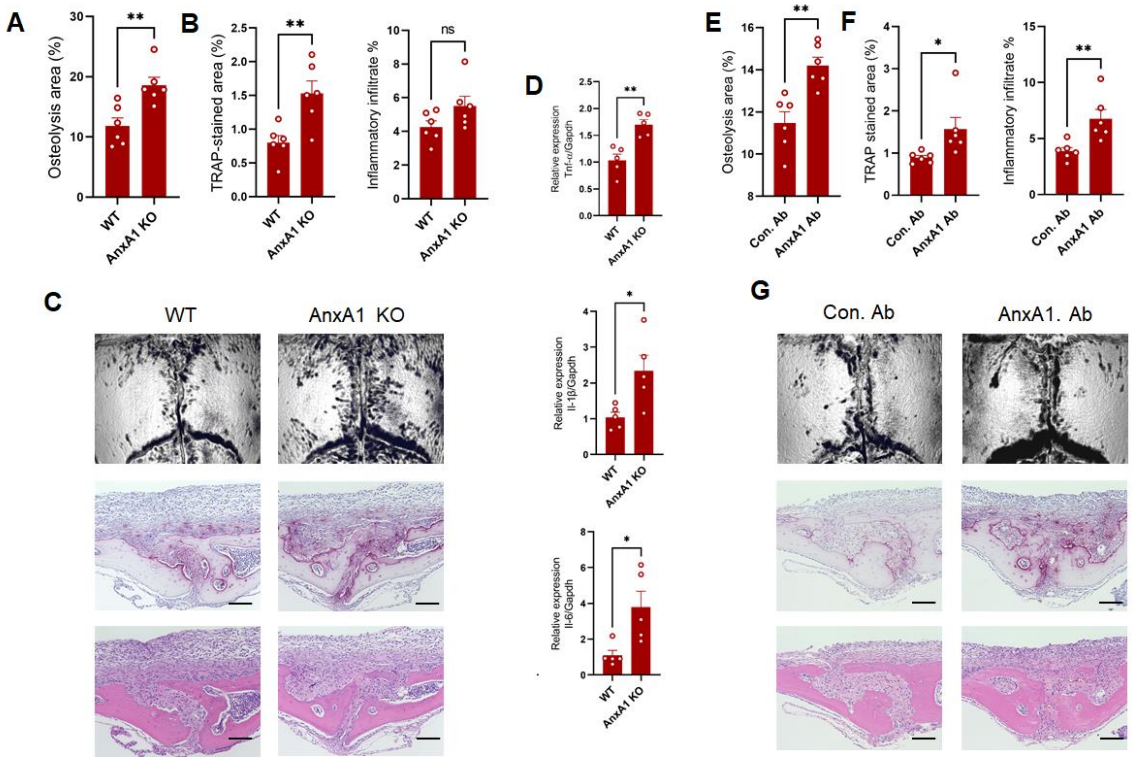

Figure 3. AnxA1 is a potential regulator of inflammatory osteolysis induced by implant wear debris. A) Quantification of the lytic area in calvarial bone tissues of AnxA1-deficient mice analyzed by micro-CT. Results represent the mean ± SEM of 6 mice. B) Quantification of TRAP-stained areas and inflammatory infiltrate in calvarial bone sections. C) Representative images for micro-CT and histological observations of bone sections stained by TRAP and H&E. D) Gene expression of inflammatory molecules in granulomatous tissue using qRT-PCR. Tissues were collected from wild type (WT) and AnxA1-defeicint mice (AnxA1 KO) after 7 days of UHMWPE debris implantation. Results represent the means of relative expression values ± SEM from 5 mice ($n = 5 \pm SEM$). Significant difference between the groups was determined by Student t-test. * $p < 0.05$, ** $p < 0.001$. E) Quantification of the lytic area in calvarial bone tissues of mice that received a function blocking antibody (AnxA1. Ab) or a control (Con. Ab) analyzed by micro-CT. F) Quantification of TRAP-stained areas and inflammatory infiltrate in calvarial bone sections of Ab-treated mice. G) Representative images for micro-CT and histological observations of bone sections stained by TRAP and H&E. Significant difference between the groups was determined by one-way ANOVA, followed by Tukey's multiple-comparison procedure. * $p < 0.05$, ** $p < 0.001$, *** $p < 0.0001$. Scale bar 100 µm.

5.3. AnxA1 represses NFκB pathway activation and promoting PPAR-γ signaling pathway.

To gain additional insights into the mechanism responsible for how AnxA1 regulates inflammation and pathological bone resorption, we first examined the effects of AnxA1 on transcription factors that are involved in the development of inflammatory responses and the differentiation of osteoclasts in human macrophage cultures. Recombinant human AnxA1 at a concentration of 100 ng/mL, suppressed the expression of phosphorylated NFκB1 (p105/50), NFκB (P65), ERK1/2, but not RelB and P38 in macrophages that had been stimulated by recombinant TNF-α and UHMWPE debris for 24h (Figure 4A, B). Furthermore, the AnxA1 treatment significantly reduced the number of TRAP-positive cells in cultured macrophages that had been stimulated with UHMWPE debris for 6 days (Figure 4C). More interestingly, the addition of AnxA1 to RANKL-stimulated human monocytes resulted in a significant decrease in the number of TRAP-positive cells and areas of bone resorption on dentine slices (Figure 4D, E). Together, these results suggest that Anxa1 acts as a potential inhibitor of osteoclastogenesis triggered by polyethylene wear debris derived from orthopedic implants. To further understand the mechanism by which AnxA1 inhibits osteoclast differentiation, human monocytes were collected from three healthy donors, stimulated by RANKL with or without AnxA1 and then subjected to RNA sequencing. The bioinformatic analysis revealed that AnxA1 reduced the expression of genes clustered in osteoclast differentiation and the NFκB pathway and enhanced the expression of genes clustered in the PPAR-γ pathway (Figure 5A). Of interest, PPAR-γ was in the list of top-regulated genes with a fold change of 7.16 (Figure 5B). The increased expression of PPAR-γ was confirmed by Western blot analysis that

showed a significant elevation in PPAR-γ expression after stimulating macrophages with AnxA1 for 180 min (Figure 5C). Bearing in mind that formyl peptide receptor 2 (FPR2) is the main receptor of AnxA1 that conveys its biological functions, we examined the increased expression of PPAR-γ in AnxA1 stimulated-macrophages pretreated with selective antagonist of FPR2 (WRW4). Of note, the ability of AnxA1 to promote expression of PPAR-γ was slightly reduced in macrophages pretreated by WRW4 (Figure 5D). These collective results suggest that AnxA1 may function as a potential suppressor of inflammation and pathological bone resorption through activating PPAR-γ pathway.

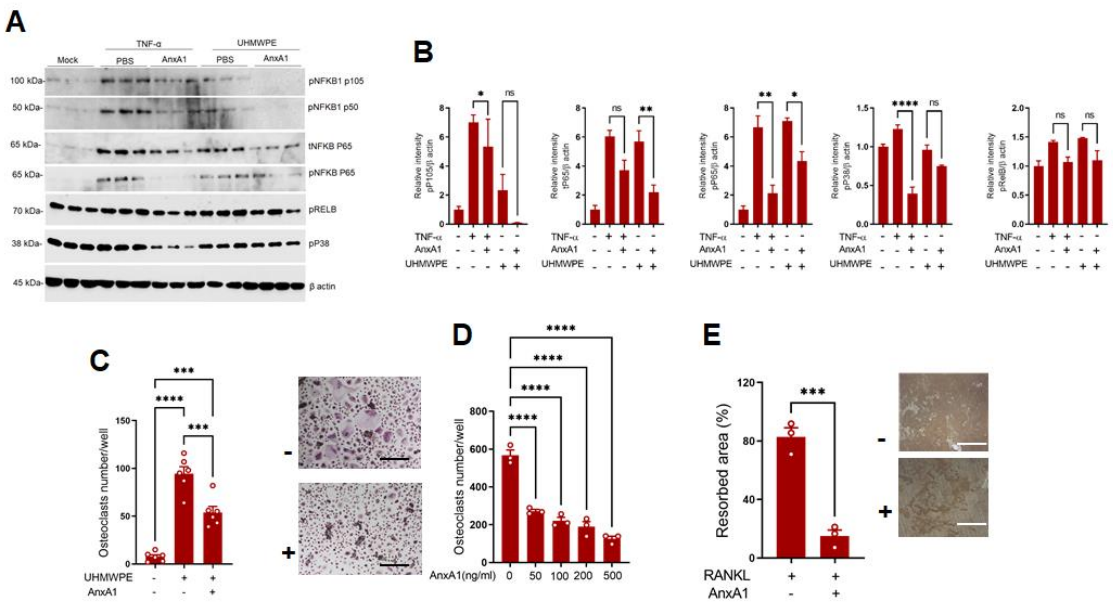

Figure 4. Effects of AnxA1 on development of inflammation and bone resorption in vitro. A) Effects of AnxA1 of the expression of transcriptional factors involved in inflammation and osteoclast differentiation. **B**) Quantification of relative intensity of bands detected by Western blotting. Detected bands for each target were subjected to ImageJ for quantification of intensities. **C**) Inhibitory effects of AnxA1 on osteoclast formation in macrophages stimulated with UHMWPE debris. Right panel shows representative images for stained osteoclasts by TRAP. Scale bars are 100 µm. **D, E**) Inhibitory effects of AnxA1 on osteoclast differentiation and bone resorption. Macrophages were stimulated with RANKL in the presence of different concentrations of AnxA1. **E**) Quantification of bone resorption area (pitting) formed by RANKL-

stimulated macrophages in a 100 ng/mL concentration of AnxA1 in bone resorption assay. Scale bars are 200 µm. Significance presents * $p < 0.05$, * $p < 0.05$, ** $p < 0.001$, *** $p < 0.0001$.

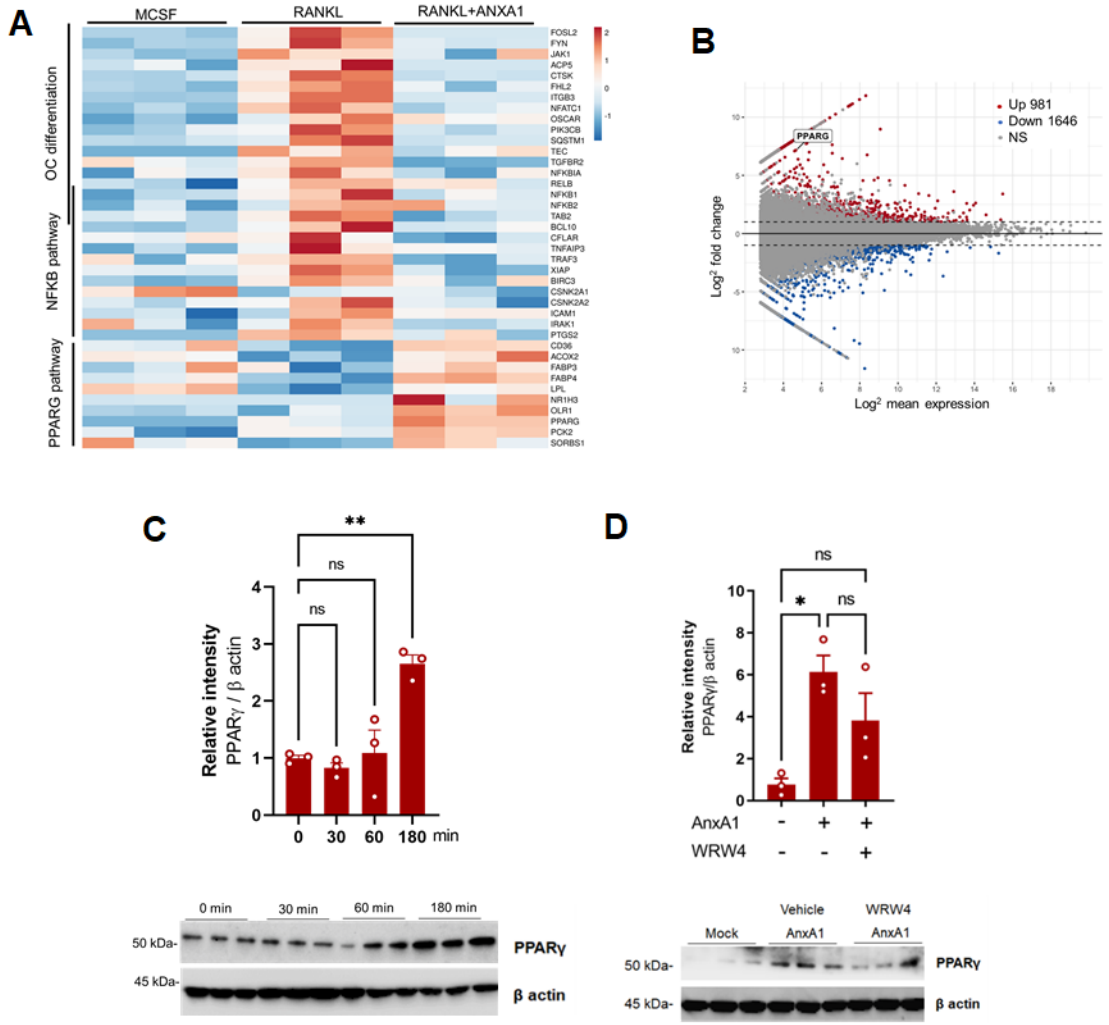

Figure 5. Molecular regulatory function of AnxA1 in inflammation and pathological bone resorption. A) Heat map based on a KEGG pathway enrichment analysis for upregulated genes in macrophages stimulated with RANKL and AnxA1. **B**) MA plot analysis for transcript expression levels of significantly up-or down-regulated genes in macrophages stimulated with RANKL and AnxA1 ($p < 0.05$) ($n = 3$). **C**) Detection of PPAR-γ by Western blot analysis in macrophages stimulated with AnxA1 at different time points. Left panel shows the quantification of the relative intensity of the detected bands ($n = 3$). D) Effects of WRW4 treatment on the expression of PPAR-γ in macrophages stimulated with AnxA1. Human macrophages were pretreated with WRW4 (1µM) for 30 min before stimulation with AnxA1. Significant difference between the groups was determined by one-way ANOVA, followed by Tukey's multiple-comparison procedure. ns, not significant. ** $p < 0.001$. * $p < 0.05$.

5.4.Protective effects of AnxA1 on cells in periprosthetic tissues.

Given the vital role of fibroblasts and osteoblasts in the development of periprosthetic osteolysis triggered by particulate wear debris, we further evaluated the effects of AnxA1 on these cells in vitro. It is noteworthy that the expression of inflammatory mediators in synoviocytes stimulated with TNF-α were significantly suppressed by AnxA1 (Figure 6A). Likewise, the Anxa1 treatment significantly enhanced the expression of the osteoblast-anabolic factors in osteoblasts that had been stimulated with TNF-α (Figure 6A). These results demonstrate that AnxA1 exerts beneficial effects on a variety of cell types at the inflammation sites.

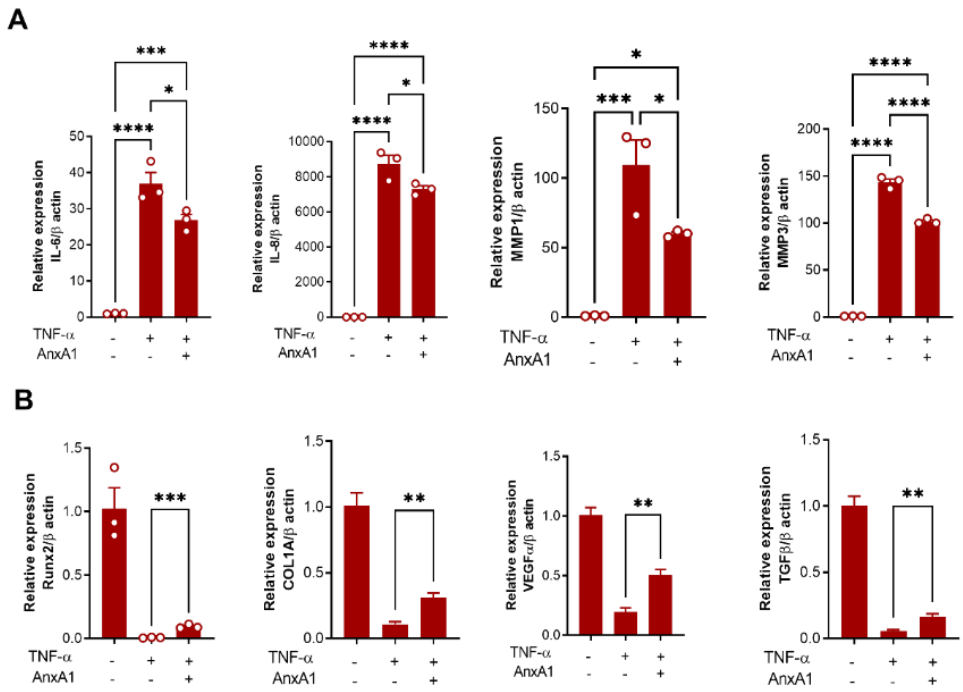

Figure 6. Effects of recombinant AnxA1 on the stimulated-FLS and osteoblasts. AnxA1 inhibits the expression of inflammatory cytokines and bone anabolic factors in human FLS (A) and osteoblasts (B) stimulated by TNF-α. Results represent the means of relative expression values ± SEM from triplicates. Significant difference between the groups was determined by one-way ANOVA, followed by Tukey's multiple-comparison procedure. * $p < 0.05$, ** $p < 0.001$, *** $p < 0.0001$, **** $p< 0.00001$. Experiments were repeated at least twice with similar results for reproducibility of data.

5.5.Pharmacological potentials of AnxA1 in periprosthetic osteolysis.

Given the fact that the AnxA1 N-terminal derived peptide Ac2-26 exerts pro-resolving properties the same as full-length AnxA1 in numerous inflammatory disease models, we assessed the therapeutic effect of the mimetic peptide Ac2-26 for treating periprosthetic osteolysis using murine experimental models. UHMWPE particles were implanted onto calvarial bone tissues and Ac2-26 was locally injected for 5 consecutive days. The other two groups of mice were treated with BML111, a selective agonist of formyl peptide receptor 2 (FPR2) for 5 consecutive days or with WRW4, a selective antagonist of FPR2, on days 1, 3, and 5. Interestingly, the mice that received Ac2-26 showed a significantly decreased bone osteolytic lesions, TRAP-staining and inflammation compared to control mice injected with vehicle (Figure 7A-D). In these mice, the gene expression of inflammatory cytokines was significantly reduced in granulomatous tissue around UHMWPE particles (Figure 7E). In contrast, neither the BML111 nor the WRW4 treatment altered/exacerbated the osteolytic lesions induced by UHMWPE particles (Figure 7A-C). These results highlight the conclusion that AnxA1 N-terminal peptide Ac2-26 may offer a novel therapeutic agent for periprosthetic osteolysis triggered by polyethylene particles.

To gain further insights into the therapeutic mechanism of Anxa1, mice that received UHMWPE particles implantation were treated with Ac2-26 mimetic peptide and a PPAR-γ antagonist (GW9662). Remarkably, the therapeutic effects of Ac2-26 were abrogated in mice that had received GW9662 (Figure 8A-D), suggesting a correlation between the therapeutic mechanism of Anxa1 and the activation of the PPAR-γ pathway. Consistently, the elevated expression of inflammatory cytokines noted in granulomatous tissue around

the UHMWPE particles in GW9662-treated mice was accompanied by a reduction in the expression of PPAR-γ (Figure 8E).

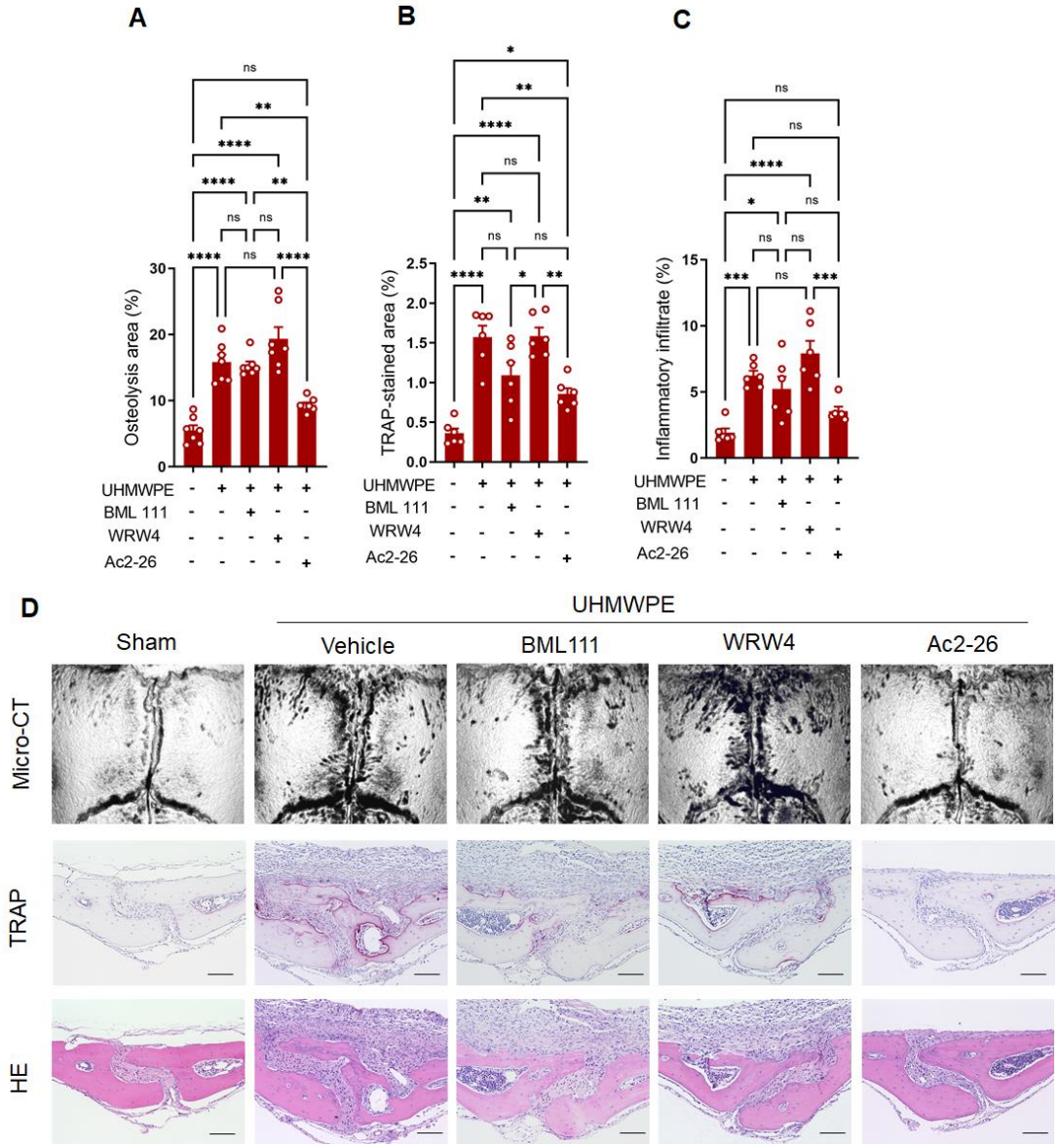

Figure 7. Therapeutic effect of Ac2-26 in UHMWPE debris-induced inflammatory osteolysis model. Debris was implanted and the calvarial bone of mice were then treated with BML111 (1mg/kg), WRW4 (2.5mg/kg) and Ac2-26 (1mg/kg). **A**) Quantification of the lytic area in calvarial bone tissues analyzed by micro-CT. Results represent the mean ± SEM of 7 mice. **B, C**) Quantification of TRAP-stained areas and inflammatory infiltrate in calvarial bone tissues. Significant difference between the groups was determined by one-way ANOVA, followed by Tukey's multiple-comparison procedure. * $p < 0.05$, ** $p < 0.001$, *** $p < 0.0001$, **** $p < 0.00001$. **D**) Representative images for micro-CT and histological observations of bone sections stained by TRAP and H&E. Scale bar 100 µm.

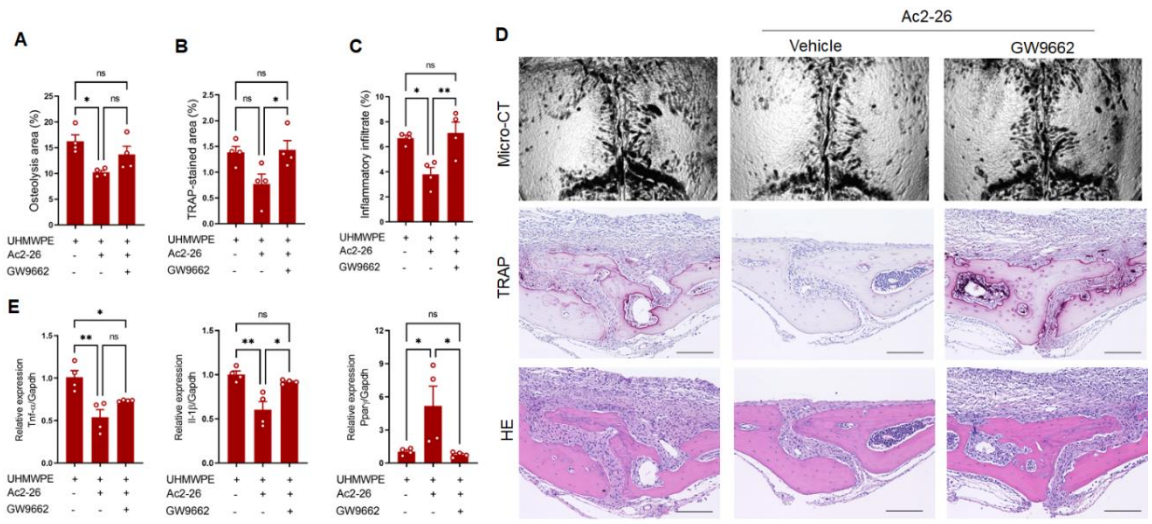

Figure 8. Treatment with aPPAR-γ antagonist impaired the therapeutic effect of Ac2-26 in a UHMWPE debris-induced inflammatory osteolysis model. A) Quantification of the lytic area in calvarial bone tissues analyzed by micro-CT. **B, C**) Quantification of TRAP-stained areas and inflammatory infiltrate in calvarial bone tissue. **D**) Representative images for micro-CT and histological observations of bone tissues stained by TRAP and H&E. Scale bars 100 µm. **E**) Gene expression of inflammatory molecules in granulomatous tissue that was formed around UHMWPE debris as analyzed by qRT-PCR. Results represent the mean ± SEM of 4 mice. Significant difference between the groups was determined by one-way ANOVA, followed by Tukey's multiple-comparison procedure. * $p < 0.05$, ** $p < 0.001$.

5.6.Pharmacological potentials of AnxA1 in other bone resorption-related diseases.

To obtain further evidence on the potential therapeutic applications of AnxA1 in pathological bone resorption related diseases, TNF-α- and RANKL-induced bone loss models were treated with Ac2-26 mimetic peptide. Treatment with the Ac2-26 peptide resulted in a significant reduction in bone loss and TRAP-stained areas in both models (Fig. 8A, B). Moreover, this treatment significantly suppressed the infiltration of inflammatory cells in the inflammatory osteolysis model induced by TNF-α (Fig. 7A-D). From these results we conclude that AnxA1 can inhibit the pathological bone resorption induced by TNF-α- and RANKL, known as the main osteoclastogenic factors in periprosthetic osteolysis.

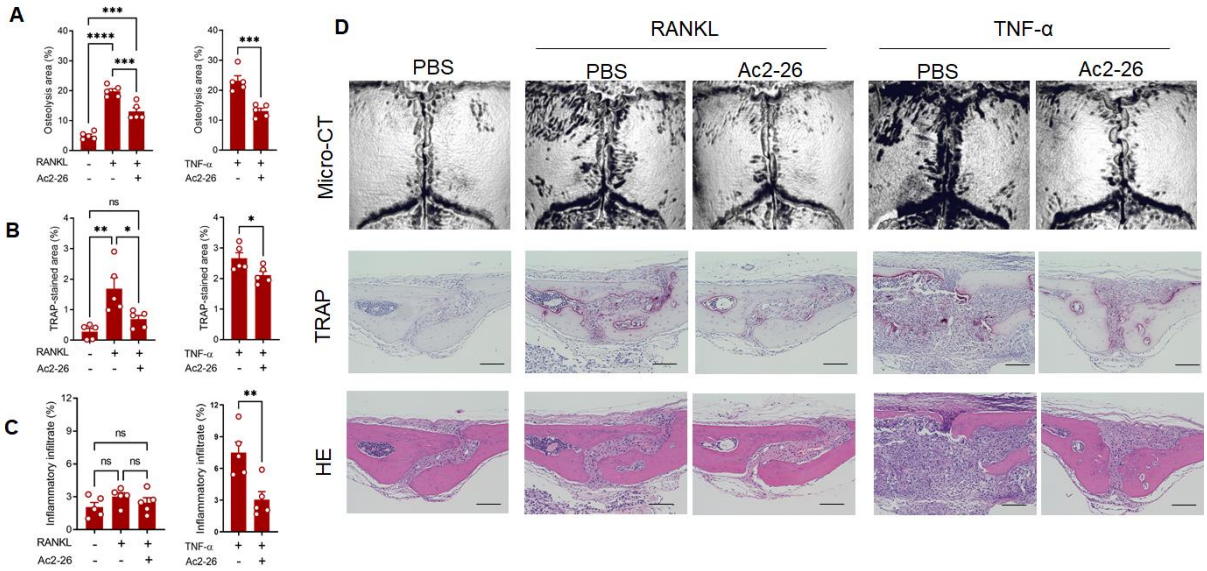

Figure 9. Therapeutic effect of Ac2-26 on pathological bone loss induced by TNF-α and RANKL administrations. Calvarial bones were locally injected with cytokines for 4 days and bone erosion was then quantified on day 5. A) Quantification of the lytic area in calvarial bone tissues analyzed by micro-CT. Results represent the mean ± SEM of 5 mice. B, C) Quantification of TRAP-stained areas and inflammatory infiltrate in calvarial bone sections. Significant difference between the groups was shown as * $p < 0.05$, ** $p < 0.001$, *** $p < 0.0001$, **** $p < 0.00001$. D) Representative images for micro-CT and histological observations of bone sections stained by TRAP and H&E. Scale bar 100 µm.

5.7. Development of injectable thermosensitive hydrogel containing AnxA1 A2-26 peptide for treatment of pathological bone resorption associated with inflammation

Given the clinical relevance of these findings, we developed an Ac2-26-mixed matrigel that allowed the locally controlled release of the peptide onto the calvarial bone and evaluated this in the TNF-induced bone loss model. Matrigel is a natural hydrogel that has been successfully used to study cell migration, angiogenesis, and protein/peptide delivery. The peptide was formulated into a thermo-responsive material that is soluble at lower temperature but turns into a semi-solid hydrogel in situ in response to the normal body temperature in vivo (37 °C) (Figure 10A). The desired formulation would be expected to produce a controlled-release pattern for the peptide through a time span of one week and to therefore maintain a sustained and prolonged effect (Figure 10A, B). Of note, a single administration of the Ac2-26-mixed Matrigel onto calvariae (beyond lambdoid suture) alleviated osteolytic lesions and the pathological bone resorption induced by the TNF-α administrations (Figure 10C-G). The results obtained from the Matrigel treatment were comparable to these for a treatment with the mimetic peptide Ac2-26 for 4 consecutive days. These collective data demonstrate the potential therapeutic and translatable applications of AnxA1 in periprosthetic osteolysis and pathological bone resorption-related diseases.

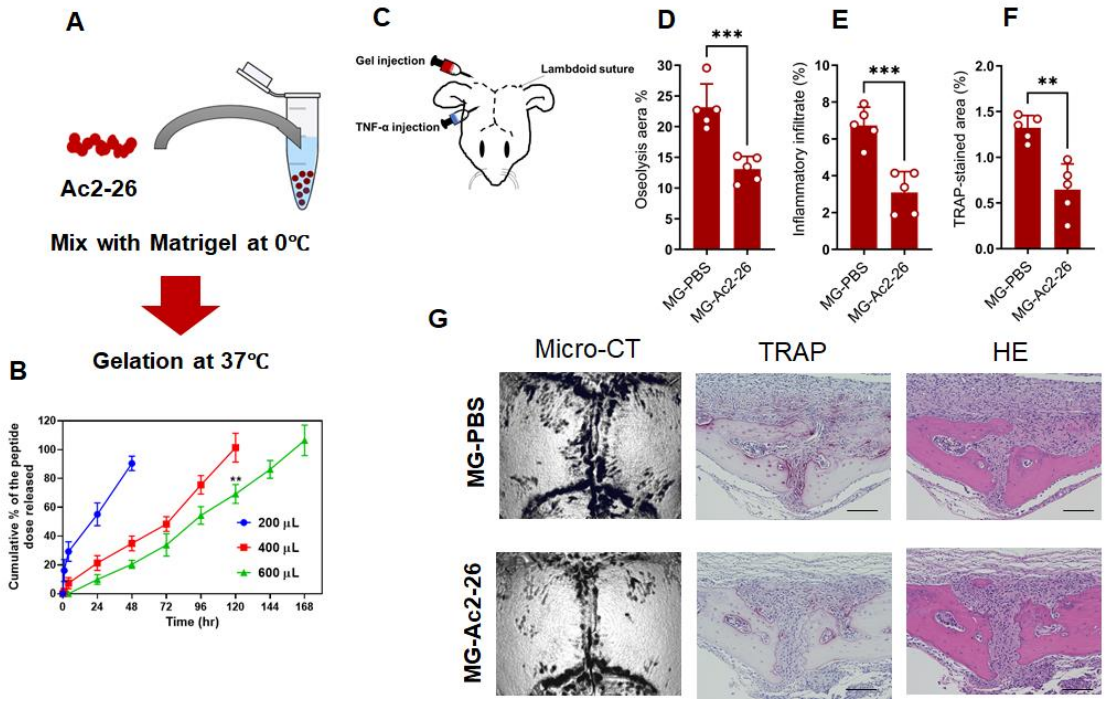

Figure 10. Matrigel encapsulating Ac2-26 and its pharmacological potential for the treatment of pathological bone resorption induced by TNF-α. A) Schematic diagram showing the procedure for preparing the Matrigel encapsulating the Ac2-26 peptide. **B**) In vitro release of the peptide from hydrogels containing different amounts of Matrigel at 37 °C and pH 7.4. The results represent the mean ± SEM of independent experiments. **p < 0.001 Significance was determined by the Two-tailed student T-test. **C**) Schematic diagram for the injection of gel and cytokines. **D-G**) Therapeutic effect of Matrigel encapsulating Ac2-26 in a bone loss model induced by TNF-α administration. The MG-PBS was the control gel, and the MG-Ac2-26 is test gel. **D**) Quantification of lytic area in calvarial bone tissues analyzed by micro-CT. **E, F**) Quantification of TRAP-stained areas and inflammatory infiltrate in calvarial bone tissues. Significant difference between groups was determined by the Student t-test. * p < 0.05, ** p < 0.001, *** p < 0.0001. Results represent the mean ± SEM of 5 mice. **G**) Representative images for micro-CT and histological observations of bone sections stained by TRAP and H&E. Scale bar 100 μm.

6. Discussion

Despite the recent advances made in our understanding of the complex cellular and molecular network underlying the pathogenesis of periprosthetic osteolysis, many questions concerning the mechanism of such disease remain unanswered. Promoting the resolution of inflammation associated with periprosthetic osteolysis represents a promising strategy for the treatment since this process is a fundamental mechanism for restoring tissue homeostasis. Therefore, I explored the pro-resolving function of AnxA1 in periprosthetic osteolysis and assessed its therapeutic application in experimental periprosthetic osteolysis models.

AnxA1 was expressed at high levels in macrophages and neutrophils within the tissues around the loosening implant. These were supported by the further findings demonstrating that the deletion of or the blocking of AnxA1 resulted in severe osteolytic lesions in murine wear debris-induced osteolysis model. Recombinant AnxA1 exhibited inhibitory effects on the inflammatory response of macrophages and RANKL-induced osteoclast differentiation through reducing the expression of NFκB transcription factor. These findings appear to be consistent with finding reported in an earlier study showing the suppressive activity of AnxA1 on inflammation and osteoclast formation in an arthritis model (Kao W et al., 2014). It is noteworthy that macrophages that had been treated with AnxA1 exhibited an elevation in the expression of PPAR-γ and a reduction in the NFκB signaling pathway. In line with these findings, the activation of PPAR-γ has been reported to be a promising approach for the treatment of inflammatory diseases and cancer through reducing NFκB p65 transcriptional activity (Hou Y et al., 2012; Bouhlel MA et al., 2007). In addition, the activation of PPAR-γ drives the polarization of monocytes to M2 macrophages with anti-inflammatory properties and inhibits RANKL-

and TNF-α-mediated osteoclast differentiation (Bouhlel MA et al., 2007; Chan BY et al., 2007; Hounoki H et al., 2008). In a related study, IL-4 was reported to inhibit RANKL-induced osteoclast formation though the activation of PPAR-γ and suppressing the activation of the NFκB pathway (Bendixen AC et al., 2001). Therefore, the possible inhibitory effects of AnxA1 might be due to its ability to decrease the activation of NFκB signaling, known as a positive regulator of the pro-inflammatory function of macrophages and the bone resorbing function of osteoclasts. Inhibition and gene deletions experiments revealed that the activation of NFκB is a central mediator of chronic inflammatory diseases, including inflammatory bowel diseases, rheumatoid arthritis, and asthma. The canonical NFκB pathway includes the activation of two catalytic subunits of IKKα and IKKβ, and the regulatory subunit of IKKγ (NEMO). IKK phosphorylates IκBα leading to IκBα degradation in proteasomes, resulting in the rapid nuclear translocation of inducible transcription factors including NF-κB1 (p100/50), NF-κB2 (p52), RelA (p65), RelB and c-Rel, which is associated with the induction of a large number of inflammatory genes. Similarly, IKKβ activity is involved in RANKL signaling in osteoclast precursors leading to the differentiation of macrophages into the osteoclasts (Ruocco MG et al., 2005). Gene manipulation experiments highlight the essential role of IKKβ in the development of inflammatory and osteoclastogenesis. Therefore, NF-κB inhibitors, namely these targeting the IKK protein family, have shown great potential for treating inflammatory diseases and bone diseases associated with impaired bone-remodeling processes such as rheumatoid arthritis and inflammatory osteolysis (Sun SC et al., 2013; Lin TH et al., 2014; Gilmore TD et al., 2011).

The therapeutic effects of AnxA1 against inflammatory osteolysis were evident both in vitro and in vivo models. These results showed that AnxA1 suppressed local

inflammatory responses, immune cell infiltration, and bone resorbing osteoclast activity in calvarial osteolysis models. AnxA1 is abundantly present in inflammatory exudates and is known to act as an anti-inflammatory mediator through activating the pro-resolving phase receptor FPR2. AnxA1 is member of the annexin superfamily of calcium-dependent phospholipid-binding proteins that is abundantly expressed in neutrophils and other innate immune cells and functions as an inflammation-resolving molecule through directing leukocyte phagocytosis, differentiation, migration, and apoptosis. AnxA1 is able to turn on c-Jun N-terminal kinase (JNK)-signaling leading to the production of IL-10 and can also enhance TGF-β signaling via promoting Smad activity (Cooray SN et al., 2013; de Graauw PD et al., 2010). These actions result in a decrease in the production of inflammatory cytokines and redirects the polarization of macrophages towards an anti-inflammatory M2 phenotype, favoring a resolving/repair phase in the tissue (Mirsaeidi M et al., 2016). In a related study, McArthur et al., in 2020, reported that the AnxA1/AMPK axis as an important pathway for inducing the production of the pro-resolving macrophage phenotype required for skeletal muscle injury regeneration (McArthur S et al., 2020). In support of this concept, AnxA1 knockout mice have demonstrated severe pathological damages in affected tissues associated with increased inflammatory responses and high levels of phosphorylated ERK-1/2 and NF-κB p65 (Yang YH et al., 2009). It is also noteworthy that PPAR-γ activation by rosiglitazone exerts pharmacological effects against alcoholic fatty livers in mice by modulating the activity of AMPK, suggesting the existence of a correlation between PPAR-γ and AMPK signaling (Shen Z et al., 2010). Consistent with this view, resolvin D1, the activation of a related pro-resolving molecule activation inhibits inflammation and the NF-κB signaling pathway in a mechanism that is dependent on PPAR-γ activation (Xia H et al., 2019).

These findings provide an explanation for the loss of the therapeutic effects of AnxA1 after injecting a PPAR-γ antagonist in wear debris-induced osteolysis model. These collective data indicate that the AnxA1/PPAR-γ signaling pathway may a play regulatory role in periprosthetic osteolysis by attenuating the inflammation and pathological bone resorption induced by implant wear debris.

The therapeutic potentials of AnxA1 and its peptide Ac2–26 have also been extensively demonstrated in experimental models, such as in allergic conjunctivitis, and in ischemic stroke models (Solito E et al., 2000; Senchenkova EY et al., 2019; Dufton N et al., 2010). The pharmacological properties of AnxA1 and its peptide Ac2–26 are known to be dependent on their ability to activate FPR2 signaling which makes it a promising anti-inflammatory and pro-resolving therapeutic target for controlling chronic inflammatory diseases. However, there is a line of evidence to suggest that Ac2–26 inhibits cell adhesiveness and migration via downmodulating α4β1 integrin and their affinity and valency, without changing their cell surface expression (Solito E et al., 2000). Likewise, AnxA1 protects the cerebrum from thromboinflammation through reducing the levels of proinflammatory cytokines and regulating the adhesion/aggregation of leukocytes and platelets to cerebral microvascular endothelial cells (Senchenkova EY et al., 2019).Therefore, it is possible that the therapeutic effects of Ac2–26 in inflammatory osteolysis might be due to its ability to reduce integrin-dependent monocyte adhesion and the migration necessary for the development of inflammation and osteoclast formation (Schneider et al., 2011). These promising findings regarding the potential therapeutic use of AnxA1 have stimulated the development of controlled-release hydrogels containing the Ac2-26 mimetic peptide. A nanomedicine approach has the potential for clinical translation in medicine, since it protects short peptides from proteolysis in vivo and

facilitates the delivery to injury sites without the need to repeat the injection. Treatment with Matrigel containing Ac2-26 caused a significant reduction in pathological bone resorption and inflammation. The obtained results were comparable to the results for the mimetic peptide treatment, which confirmed the use of Ac2-26 in the treatment of periprosthetic osteolysis and pathological bone resorption-related diseases. A similar approach was successfully developed for dermal wound repair applications with an optimal controlled release formulation of Ac2-26 (Gaudio PD et al., 2015). Moreover, nanoparticles that allow the slow release of Ac2-26 was reported to reduce tissue damage in zymosan-induced peritonitis and protect against advanced atherosclerosis in hypercholesterolemic mice (Fredman G et al., 2015). Further study including development of safer nanomaterials for the delivery of Ac2-26 promise to have great potential in clinical applications.

7. Conclusions

Periprosthetic osteolysis is the most common cause of arthroplasty failure and there is no available therapy yet. The present study sheds light, for the first time, on the functional and cellular association between neutrophils and the pathophysiology of inflammatory osteolysis, delineating new strategies for innovative therapeutic approaches for preventing implant failure. The AnxA1/PPAR-γ axis appears to play an important role in attenuating inflammation and pathological bone resorption in periprosthetic osteolysis (Figure 11). This study highlights AnxA1 as clinically-translatable therapeutic agent for the prevention of implant loosening.

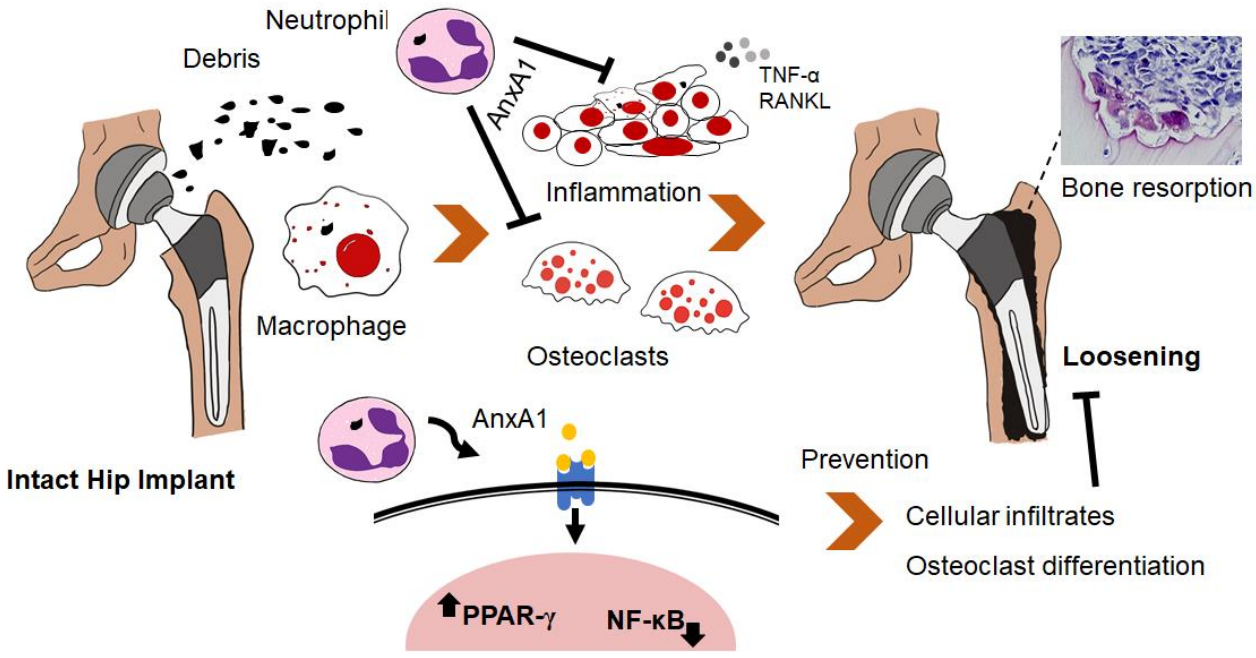

Figure 11. Schematic summary and conclusions of the current study.

Acknowledgements

This work was carried out at the Frontier Research Center for Advanced Material and Life Science, Department of Orthopedic Surgery, Faculty of Medicine and Graduate School of Medicine, Hokkaido University. Knockout mice (AnxA1 KO mice) were generated at the Laboratory Animal Resource Center, University of Tsukuba. This work was supported by Grant-in-Aid for Scientific Research C (17 K10993) from Japan Society for the Promotion of Science, and grants from Akiyama Life Science Foundation, Kobayashi Foundation, Uehara Memorial Foundation.

I am deeply indebted to Prof. Norimasa Iwasaki my supervisor at the Department of Orthopedic Surgery for accepting me in his laboratory, and for his intellectual guidance, constructive criticism, invaluable suggestions and his great support throughout the period of my study. My deepest thanks are expressed to advisor Assistant Prof. M. Alaa Terkawi for his advice, guidance, precious comments, encouragement and great support. I extend my gratitude to Associate Profs. Ken Kadoya, Daisuke Takahashi and Tomohiro Shimizu for the helpful guidance, advice and comments.

My sincere thanks are also to Dr. Keita Uetsuki and Mrs. Tomoyo Yutani from Teijin Nakashima Medical Co., Ltd. (Japan) for providing UHMWPE particulate debris from their hip implant materials. I also thank Dr. Fayna Garcia-Martin and Mr. Chowdhury Arpan (Graduate School and Faculty of Advanced Life Science, Laboratory of Advanced Chemical Biology, Hokkaido University) for their help in the synthesis and characterization of the peptide Ac2-26. I thank Dr. Mahmoud M. Abd Elwakil, Mahmoud A. Younis and Porf. Hideyoshi Harashima (Laboratory of Innovative Nanomedicine, Faculty of Pharmacy and Pharmaceutical Sciences, Hokkaido University) for their help in the synthesis of hydrogel.

I would like to thank all my colleagues at the Musculoskeletal and Immunological Research Unit (MIRU), namely Dr. Gen Matsumae, Dr. Taku Ebata, Dr. Shunichi Yokota and Dr. Yoshio Nishida, as well as all members in our department for their support, assistance, and friendship. Finally, I would like to thank my family for great support patience and all animals I have used for my experiments.

Disclosure of Conflict of Interest

The author declares no conflict of interest

References

Bala, A., Ivanov, D.V., Huddleston, J.I 3rd., Goodman, S.B., Maloney, W.J., Amanatullah, D.F. (2020). The Cost of Malnutrition in Total Joint Arthroplasty. J Arthroplasty. *35*(4):926-932.e1.

Bendixen, A.C., Shevde ,N.K., Dienger ,K.M., Willson ,T.M., Funk, C.D., Pike, J.W. (2001). IL-4 inhibits osteoclast formation through a direct action on osteoclast precursors via peroxisome proliferator-activated receptor gamma 1. Proc Natl Acad Sci U S A. *27*,98(5):2443-8.

Bouhlel, M.A. et al. (2007). PPARγ activation primes human monocytes into alternative M2 macrophages with anti-inflammatory properties. Cell Metab. *6*(2):137–43.

Buckley, C.D., Gilroy, D.W., Serhan, C.N., (2014). Proresolving lipid mediators and mechanisms in the resolution of acute inflammation. Immunity. *40,* 315–327.

Chakravarti, A., Raquil, M .A., Tessier , P., Poubelle, P .E. (2009). Surface RANKL of Toll-like receptor 4-stimulated human neutrophils activates osteoclastic bone resorption. Blood. *20*:114(8), 1633-1644.

Chan, B.Y. et al. (2007). PPAR agonists modulate human osteoclast formation and activity in vitro. Bone. *40*(1):149-59.

Charnley, J. (1961). Arthroplasty of the hip. A new operation. Lancet. *1*, 1129–1132.

Cobelli, N., Scharf, B., Crisi, G.M., Hardin, J., Santambrogio, L. (2011). Mediators of the inflammatory response to joint replacement devices. Nat Rev Rheumatol. *10*: 600-608.

Cooray, S.N., et al. (2013). Ligand-specific conformational change of the G-protein-coupled receptor ALX/FPR2 determines proresolving functional responses. Proc Natl Acad Sci U S A. *110*: 18232–18237.

de Graauw, M., et al. (2010). Annexin A1 regulates TGF-beta signaling and promotes metastasis formation of basal-like breast cancer cells. Proc Natl Acad Sci U S A. *107*: 6340–6345.

Dufton, N., et al. (2010). Anti-inflammatory role of the murine formyl-peptide receptor 2: ligand-specific effects on leukocyte responses and experimental inflammation. J Immunol. *184*(5):2611-2619.

Fredman, G., et al., (2015). Targeted nanoparticles containing the proresolving peptide Ac2-26 protect against advanced atherosclerosis in hypercholesterolemic mice. Sci Transl Med. *275*(7): 4;7(277):277er2.

Fullerton, J., Gilroy., D. (2016). Resolution of inflammation: a new therapeutic frontier. Nat Rev Drug Discov. *15,* 551–567.

Gaudio, P.D., et al. (2015). Evaluation of in situ injectable hydrogels as controlled release device for ANXA1 derived peptide in wound healing. Carbohydr Polym. *115*: 629–633.

Gavins, F.N., Hickey, M.J. (2012). Annexin A1 and the regulation of innate and adaptive immunity. Front Immunol. *3,* 354.

Gilmore, T.D., Garbati, M.R. (2011). Inhibition of NF-kappaB signaling as a strategy in disease therapy. Curr Top Microbiol Immunol. 349:245–263.

Headland, S.E., et al. (2015). Neutrophil-derived microvesicles enter cartilage and protect the joint in inflammatory arthritis. Sci Transl Med. *7*(315):315ra190.

Hou, Y., Moreau, F., Chadee, K. (2012). PPARγ is an E3 ligase that induces the degradation of NFκB/p65. Nat. Commun. *3*:1300.

Hounoki, H., et al. (2008). Activation of peroxisome proliferator-activated receptor gamma inhibits TNF-alpha-mediated osteoclast differentiation in human peripheral

monocytes in part via suppression of monocyte chemoattractant protein-1 expression. Bone. *42*(4):765-74.

Ito, S., Matsumoto, T., Enomoto, H., Shindo, H. (2009). Histological analysis and biological effects of granulation tissue around loosened hip prostheses in the development of osteolysis. J Orthop Sci. *9*: 478-487.

Kamaly, N., et al. (2013). Development and in vivo efficacy of targeted polymeric inflammation-resolving nanoparticles. Proc Natl Acad Sci USA. *110*(16): 6506–6511.

Kandahari, A.M., Yang, X., Laroche, K.A., Dighe, A.S., Pan, D., Cui, Q. (2016). A review of UHMWPE wear-induced osteolysis: the role for early detection of the immune response. Bone Res. *4*: 16014.

Kao, W., Gu, R., Jia, Y., et al. (2014). A formyl peptide receptor agonist suppresses inflammation and bone damage in arthritis. Br J Pharmacol. *171*(17):4087-4096.

Lin, T.H., et al. (2014). Chronic inflammation in biomaterial-induced periprosthetic osteolysis: NF-kappaB as a therapeutic target. Acta Biomater. *10*(1):1–10

Matsumae, G., et al. (2021). Targeting thymidine phosphorylase as a potential therapy for bone loss associated periprosthetic osteolysis. Bioeng Transl Med. *6*(3):e10232.

Matsumae, G., et al. (2022). Determination of optimal concentration of vitamin E in polyethylene liners for producing minimal biological response to prosthetic wear debris. J Biomed Mater Res B Appl Biomater. *10*(9):2182-2187.

McArthur, S., et al. (2020). Annexin A1 drives macrophage skewing to accelerate muscle regeneration through AMPK activation. J Clin Invest. *130*(3):1156-1167.

Mirsaeidi, M., Gidfar, S., Vu, A., Schraufnagel, D. (2016). Annexins family: insights into their functions and potential role in pathogenesis of sarcoidosis. J Transl Med. *14*:89.

Mócsai, A. (2013). Diverse novel functions of neutrophils in immunity, inflammation, and beyond. J Exp Med. *2010*,1283–1299.

Moutsopoulos, N.M., et al. (2014). Defective neutrophil recruitment in leukocyte adhesion deficiency type I disease causes local IL-17-driven inflammatory bone loss. Sci Transl Med.*6*(229):229ra40.

Nadkarni, S., et al. (2016). Neutrophils induce proangiogenic T cells with a regulatory phenotype in pregnancy. Proc Natl Acad Sci U S A. *113*(52): E8415-E8424.

Nathan, C. (2006). Neutrophils and immunity: challenges and opportunities. Nat Rev Immunol. *6*(3), 173-182.

Németh, T., Mócsai, A. (2012). The role of neutrophils in autoimmune diseases. Immunol. Lett. *30*;143(1), 9-19.

Papatheofanis, F. J., Barmada, R. (1991). Polymorphonuclear leukocyte degranulation with exposure to polymethylmeth-acrylate nanoparticles. J Biomed Mater Res. *25*: 761-71.

Perretti, M., Dalli, J. (2009). Exploiting the Annexin A1 pathway for the development of novel anti-inflammatory therapeutics. Br J Pharmacol. *158*(4), 936-946.

Perucci, L.O., Sugimoto, M.A., Gomes, K.B., Dusse, L.M., Teixeira, M.M., Sousa, L.P. (2017). Annexin A1 and specialized proresolving lipid mediators: promoting resolution as a therapeutic strategy in human inflammatory diseases. Expert Opin Ther Targets. *21*(9), 879-896.

Rhys, H.I., Dell'Accio, F., Pitzalis, C., Moore, A., Norling, L.V., Perretti, M. (2018). Neutrophil Microvesicles from Healthy Control and Rheumatoid Arthritis Patients Prevent the Inflammatory Activation of Macrophages. EBioMedicine. *29*:60-69.

Ritger, P.L., Peppas, N.A. (1987). A simple equation for description of solute release II. Fickian and anomalous release from swellable devices. J control Release. *5*: 37-42.

Ruocco, M.G., et al. (2005). I{kappa}B kinase (IKK){beta}, but not IKK{alpha}, is a critical mediator of osteoclast survival and is required for inflammation-induced bone loss. J Exp Med. *201*(10):1677–1687.

Schauer, C., et al. (2014). Aggregated neutrophil extracellular traps limit inflammation by degrading cytokines and chemokines. Nat Med. *20*(5):511-517.

Schneider, J.G., Amend, S.R., Weilbaecher, K.N. (2011). Integrins and bone metastasis: integrating tumor cell and stromal cell interactions. Bone. *48*(1):54-65.

Senchenkova, E.Y., et al. (2019). Novel Role for the AnxA1-Fpr2/ALX Signaling Axis as a Key Regulator of Platelet Function to Promote Resolution of Inflammation. Circulation. *23*; 140(4):319-335.

Shen, Z., et al. (2010). Involvement of adiponectin-SIRT1-AMPK signaling in the protective action of rosiglitazone against alcoholic fatty liver in mice. Am J Physiol Gastrointest Liver Physiol. *298*(3): 364–374.

Solito, E., Romero, I.A., Marullo, S., Russo-Marie, F., Weksler, B.B. (2000). Annexin 1 binds to U937 monocytic cells and inhibits their adhesion to microvascular endothelium: involvement of the alpha 4 beta 1 integrin. J Immunol. *165*(3):1573-81.

Sun, S.C., Chang, J.H., Jin, J. (2013). Regulation of nuclear factor-kappaB in autoimmunity. Trends Immunol. *34*: 282–289.

Terkawi, M.A., et al. (2019). Identification of IL-27 as potent regulator of inflammatory osteolysis associated with vitamin E-blended ultra-high molecular weight polyethylene debris of orthopedic implants. Acta Biomater. *89*:242–51.

Terkawi MA, et al. (2018). Transcriptional profile of human macrophages stimulated by ultra-high molecular weight polyethylene particulate debris of orthopedic implants uncovers a common gene expression signature of rheumatoid arthritis. Acta Biomater.*65*:417–25.

Terkawi, M.A., Matsumae, G., Shimizu, T., Takahashi, D., Ken, K., Iwasaki, N. (2022). Interplay between inflammation and pathological bone resorption: Insights into recent mechanisms and pathways in related diseases for future perspectives. Int J Mol Sci. *23*(3):1786.

Tian, Y., et al. (2020). Blockade of XCL1/Lymphotactin Ameliorates Severity of Periprosthetic Osteolysis Triggered by Polyethylene-Particles. Front Immunol. *11*:1720.

Wozniak, W., Markuszewski, J., Wierusz-Kozlowska, M., Wysocki, H. (2004). Neutrophils are active in total joint implant loosening. Acta Orthop Scand. *75*(5):549-553.

Xia, H., et al. (2019). Resolvin D1 Alleviates Ventilator-Induced Lung Injury in Mice by Activating PPAR*γ*/NF-*κ*B Signaling Pathway. Biomed Res Int. *2019*:6254587.

Yang, Y.H., Aeberli, D., Dacumos, A., Xue, J.R., Morand, E.F. (2009). Annexin-1 regulates macrophage IL-6 and TNF via glucocorticoid-induced leucine zipper. J Immunol. *15*;183(2):1435-45.

Yokota, S., et al. (2021). Cardiotrophin Like Cytokine Factor 1 (CLCF1) alleviates bone loss in osteoporosis mouse models by suppressing osteoclast differentiation through activating interferon signaling and repressing the nuclear factor-κB signaling pathway. Bone. *153*:116140.